Major Project Report on

"SHEAR AND DILATION BEHAVIOR OF ROCK-JOINTS"

Submitted in Partial Fulfilment for the Award of the Degree of

MASTERS OF TECHNOLOGY

IN

CIVIL ENGINEERING

With Specialisation in

GEOTECHNICAL ENGINEERING

By

Reena Negi

(Roll No. 06/GTE/2k10)

Under The Guidance of

Mr. A.K. Shrivastava

Asst. Professor

Department of Civil and Environmental Engineering

Delhi Technological University, Delhi

2010-2012

DELHI TECHNOLOGICAL UNIVERSITY

CERTIFICATE

This is to certify that the project report entitled "SHEAR AND DILATION BEHAVIOUR OF ROCK JOINTS", is a bona fide record of work carried out by Reena Negi (06/GTE/2k10) under my guidance and supervision, during the academic session 2010-2012 in partial fulfilment of the requirement for the degree of Master of Technology in Geotechnical Engineering from Delhi Technological University, Delhi.

To the best of my knowledge, the matter embodied in the thesis has not been submitted to any other University/Institute for the award of any Degree or Diploma.

Mr. A. K. Shrivastava

Asst. Professor

Department of Civil Engineering

Delhi Technological University

Delhi

DELHI TECHNOLOGICAL UNIVERSITY

ACKNOWLEDGEMENT

I would like to express my deepest sense of gratitude and indebtedness to my guide and motivator **Mr. A. K. Shrivastava**, Assistant Professor, Civil Engineering Department, Delhi Technological University for his valuable guidance and support in all the phases from conceptualization to final completion of the project.

I wish to convey my sincere gratitude to **Prof. A.K. Gupta**, H.O.D, and all the faculties of Civil Engineering Department, Delhi Technological University who have enlightened me during my project.

I am deeply thankful towards all the lab assistants of my college who have helped me conducting the experiments.

I would also like to thank my parents for their encouragement and persistent support which has helped me to do better in all of my endeavours.

I sincerely thank my friends Mr. Prateek Negi, Mr. Ankur Mudgal and Ms. Prerana Yadav whose moral support made this project possible.

Last but not the least; I would like to thank all the people directly and indirectly involved in successful completion of this project.

REENA NEGI

Roll No. 06/GTE/2k10

Regn. No. DTU/MT/84

M.Tech in Geotechnical Engineering

Department of Civil and Environmental Engineering

Delhi Technological University

TABLE OF CONTENTS

Certificate ..... **i**

Acknowledgement ..... **ii**

Table of Contents ..... **iii-iv**

List of Figures ..... **v-vi**

List of Tables ..... **vii**

Abstract ..... **viii**

Notations ..... **ix**

Chapter 1: Introduction **1-4**

1.1 Introduction 2

1.2 Objective of Work 3

1.3 Organization of Report 3

Chapter 2: Literature Review **5-24**

2.1 Shear Behaviour of Rock Joint 6

2.1.1 Patton Shear Strength Criteria 6

2.1.2 Ladanyi and Archambault Shear Strength Criteria 6

2.1.3 Barton's Shear Strength Criteria 7

2.2 Dilation Behaviour of Rocks 8

2.2.1 Introduction 8

2.2.2 Model of Ladayani and Archambault 10

2.2.3 Barton and Choubey 10

2.3 Peak Shear Displacement in Rocks 12

2.4 Numerical Methods in Rock Engineering 13

2.4.1 The FDM and Related Methods 16

2.4.2 The FEM and Related Methods 18

2.4.3 The BEM and Related Methods 19

2.4.4 The DEM and Related Methods 20

2.4.5 Hybrid Models and Methods 23

Chapter 3: Rock Joint Properties **25-32**

3.1 Uniaxial Compressive Strength (UCS) 26

3.2 Joint Wall Compression Strength (JCS) 27
3.3 Joint Roughness Coefficient (JRC) 28
3.4 Scale Effect on JRC and JCS 31
3.5 Joint Stiffness Characteristic 31
3.5.1 Joint Shear Stiffness 31
3.5.2 Joint Normal Stiffness 32

Chapter 4: Experimental Setup 33-56
4.1 Experimental Setup 34
4.1.1 Materials Used 34
4.1.2 Preparation of Specimens 35
4.1.2.1 UCS Test 36
4.1.2.2 Direct Shear Test 37
4.2 Material Characterization 38
4.2.1 Determination of Specific Gravity 38
4.2.2 Determination of Initial and Final Setting Time 39
4.2.3 Particle Size Distribution 40
4.2.4 UCS Test [7 day and 14 day] 40
4.2.5 Direct Shear Test [14 day] 45
4.2.5.1 Specification of Apparatus 46
4.3 Results 48
4.3.1 For 15° Asperity Angle 48
4.3.2 For 30° Asperity Angle 52
4.3.3 Discussion on Experimental Results 55

Chapter 5: Numerical Modelling 57-78
5.1 UDEC 58
5.2 Continuously Yielding Joint Model 60
5.3 Modelling of Direct Shear Test in UDEC 63
5.4 Comparison of Experimental and UDEC Result 66
5.5 Comparison of results with that of obtains using well known equation 72

Chapter 6: Conclusions 79-80

Chapter 7: Scope for Future Work 81-82

References 83-88

LIST OF FIGURES

Fig1.1: Typical shear displacement- dilation curve 9
Fig 1.2: Typical result of Direct Shear Test 10
Fig 2.3: Different Methods of Numerical Modelling 14
Fig 2.4: Suitability of different methods for an excavation in a rock mass 16
Fig 2.5: Representation of a fractured rock mass by FEM 19
Fig 2.6: Representation of a fractured rock mass by BEM 20
Fig 2.7: Representation of a fractured rock mass by DEM. 23
Fig 3.1: Roughness profile (Barton and Choubey, 1977).....29
Fig 3.2: Geometry of Asperities 30
Fig 4.1: Flow Chart of Experimental Setup 34
Fig 4.2: UCS Sample for Curing 36
Fig 4.3: Mould for sample preparation of Direct Shear Test 37
Fig 4.4: Direct Shear Test Sample 38
Fig 4.5: Particle Size Distribution Curve 40
Fig 4.6: Typical Stress- Strain curve for (a) 30%; (b) 40%; (c) 50% water by weight. 42
Fig 4.7: Typical Stress- Strain curve for 50% water by weight after 14 day curing 43
Fig 4.8: Failure Pattern Observed in samples (a) 30%; (b) 40%; (c) 50% water by weight 44
Fig 4.9: Failure Pattern Observed in samples for 50% water by weight after 14 day curing.....45
Fig 4.10: Direct Shear Testing Equipment 47
Fig 4.11: LVDT's and Loading frame in Direct Shear Test 48
Fig 4.12: Direct Shear Samples After Shearing 49
Fig 4.13: Comparison of shear and dilation behaviour of 15° asperity samples at different Normal Stress 50
Fig 4.14: Comparison of shear and dilation behaviour of 30° asperity samples at different normal Stress 51
Fig 4.15: Failure Envelope for Joints blocks 53
Fig 4.16: Comparison of Peak Shear Displacement for 15° and 30° asperity angle 54
Fig 4.17: Comparison of Peak Secant Dilation angle for 15° and 30° asperity angle 54
Fig 5.1: Shear stress- displacement curve and bounding shear strength 63
Fig 5.2: Blocks created by UDEC 64
Fig 5.3: Comparison of Experimental result with UDEC for 15° asperity angle at σ_n=0.05MPa 67
Fig 5.4: Comparison of Experimental result with UDEC for 15° asperity angle at σ_n=0.1MPa 67
Fig 5.5: Comparison of Experimental result with UDEC for 15° asperity angle at σ_n=0.2MPa 68
Fig 5.6: Comparison of Experimental result with UDEC for 15° asperity angle at σ_n=0.25MPa 68

Fig 5.7: Comparison of Experimental result with UDEC for 15° asperity angle at σ_n=0.5MPa 69
Fig 5.8: Comparison of Experimental result with UDEC for 30° asperity angle at σ_n=0.05MPa 69
Fig 5.9: Comparison of Experimental result with UDEC for 30° asperity angle at σ_n=0.1MPa 70
Fig 5.10: Comparison of Experimental result with UDEC for 30° asperity angle at σ_n=0.2MPa 70
Fig 5.11: Comparison of Experimental result with UDEC for 30° asperity angle at σ_n=0.25MPa 71
Fig 5.12: Comparison of Experimental result with UDEC for 30° asperity angle at σ_n=0.5MPa 71
Fig 5.13: Comparison of Experimental Peak Shear Stress with the results of UDEC, Barton's Eqn. and Patton's Eqn. for 15° asperity angle 73
Fig 5.14: Comparison of Experimental Peak Shear Stress with the results of UDEC, Barton's Eqn. and Patton's Eqn. for 30° asperity angle 74
Fig 5.15: Comparison of Experimental Peak Shear Displacement with the results of UDEC, Barton-Bandis Eqn. and Asadollahi's Eqn. for 15° asperity angle 75
Fig 5.16: Comparison of Experimental Peak Shear Displacement with the results of UDEC, Barton-Bandis Eqn. and Asadollahi's Eqn. for 30° asperity angle 76
Fig 5.17: Comparison of Experimental Peak dilation angle with the results of Barton's Eqn. and Asadollahi's Eqn. for 15° asperity angle 77
Fig 5.18: Comparison of Experimental Peak dilation angle with the results of UDEC, Barton-Bandis Eqn and Asadollahi's Eqn for 30° asperity angle 78

LIST OF TABLES

Table 1: Recommended model for shear stress–displacement (Barton, 1982)..... 13
Table 2: Comparison of Compressive strength for different water content after 7 day curing 42
Table 3: Experimental values obtained for 15° asperity sample 52
Table 4: Experimental values obtained for 30° asperity sample 53
Table 5: Continuously yielding model properties for direct shear tests..... 65
Table 6: Value of Peak Shear Stress obtained for 15° angle 72
Table 7: Value of Peak Shear Stress obtained for 30° angle 73
Table 8: Value of Peak Shear displacement obtained for 15° angle 75
Table 9: Value of Peak Shear displacement obtained for 30° angle 76
Table 10: Value of Peak Dilation angle obtained for 15° angle 77
Table 11: Value of Peak Dilation angle obtained for 30° angle 78

ABSTRACT

Strength characteristics of rock mass are greatly influenced by the presence of discontinuities. Intact rocks jointed in comparison of fractured rock mass shows high permeability, higher deformation characteristics and low shear strength along the plane of discontinuity. Thus the study of strength parameters becomes very important for the analysis of effect of joints on rock mass. In case of rough joint surfaces shear displacement is accompanied by vertical displacement or dilation and it is one of most important parameter which should be considered while designing any structure in jointed rocky strata. As it is very difficult to study the behaviour of actual rock joint in laboratory and field, artificial rock joint model are being used by researchers in order to estimate the behaviour of actual rocky strata.

The aim of this research is also to study the shear and dilation behaviour of artificial regular rock joint (prepared by Plaster of Paris). Samples of rock- joints are prepared at an asperity angle of 15° and 30° of Plaster of Paris at a moulding water content of 50% by weight. Direct shear tests were conducted after 14 days of air curing under CNL condition in conventional direct shear machine. Shear stress offered and dilation measured for 30° asperity sample was more than that of 15° asperity sample at the same normal stress. It has also been noted down that peak shear displacement not only increases with normal stress for same asperity angle joint but also increases with increase in asperity angle at same normal stress. UDEC (Universal Distinct Element Code) was found suitable in predicting peak shear stress when compared conventional criteria's given by Barton, 1973, Patton, 1966 as they are over predicting the results. When UDEC is compared with Barton-Bandis equation, 1981 and Asadollahi's equation, 2010 for predicting peak shear displacement it has been found that UDEC is predicting comparable values while these equation are under predicting the result.

NOTATIONS

1. $d_{s.peak}$ -peak secant dilation angle
2. $d_{t.peak}$- peak secant dilation angle
3. $d_{t.mobilized}$- mobilized dilation angle
4. JCS- Joint Compressive Strength
5. JRC-Joint Roughness Coefficient
6. L- length of rock block in shearing direction in meters
7. M- damage coefficient
8. δ_h – shear displacement in mm
9. δ_{peak} – peak shear displacement (at which shear stress is maximum) in mm
10. δ_v – dilation in mm
11. $\delta_{v.peak}$ – dilation at peak shear displacement in mm
12. φ_b- base friction angle
13. φ_r- residual friction angle
14. σ_c-uniaxial compressive strength in N/mm^2
15. σ_n- normal stress in N/mm^2
16. τ_{peak}- peak shear strength of rock joints in N/mm^2

Dedication

I dedicate this thesis

to my family, my teachers and my friends for

supporting me all the way & doing all thee

wonderful things for me.

CHAPTER 1

INTRODUCTION

1.1 Introduction

Rock mechanics has developed as a separate field of engineering. It not only deals with rocks as engineering materials but it also deals with changes in mechanical behaviour in rocks such as stress, strain and movements in rocks brought in due to engineering activities in rocky strata. It is also associated with design and stability of underground structures in rocks.

Rock mass is a discontinuous medium consisting of fractures which may exert significant influence on their engineering responses. These discontinuities may exist with or without infill material. The strength of rock masses depends on the behaviour of these discontinuities or planes of weaknesses. The frequency of joints, their orientation with respect to the engineering structures, and the roughness of the joint have a significant importance from the stability point of view. Reliable characterization of the strength and deformation behaviour of jointed rocks is very important for safe design of civil structures such as buildings, dams, bridge piers, tunnels, etc. The properties of the intact rock between the discontinuities and the properties of the joints themselves can be determined in the laboratory where as the direct physical measurements of the properties of the rock mass are very expensive and difficult.

As it is very difficult to study the behaviour of actual rock joint in lab and field, artificial rock joint model are being used for study purpose. The aim of this research is also to study the shear and dilation behaviour of artificial rock joint (prepared by Plaster of Paris) and to model the shear behaviour using experimental results and numerical methods.

Artificial joints have been studied mainly as they have the advantage of being reproducible, for example, Gypsum plaster has been found to be suitable for simulating the behaviour of jointed soft rocks such as coal, friable limestone, clay shale and mudstone.

Laboratory studies show that many different failure modes are possible in jointed rock and that the internal distribution of stresses within a jointed rock mass can be highly complex. Numerical simulation of rock joints has been also been performed by researcher time to time (Indratna et.al, 1999; Roosta et.al., 2006; Shrivastava et.al. 2012) and it has been observed by them that numerical results are in close approximation to experimental results.

1.2 Objective of the Work

The present study aims to analyze the effect of asperity profile and normal load on shearing behaviour of jointed rock sample and to check the applicability of UDEC in predicting the shear behaviour. In order to design any structure on rocky strata, for constructing tunnel or for slope stability analysis one needs to thoroughly study the behaviour of rock joints. Also obtaining jointed sample and conducting shear test on it is very tedious, difficult and expensive too therefore here shear test are conducted on artificial jointed sample. This also aims to study the effect of asperity angle or roughness profile and normal load on peak shear stress, peak shear displacement and dilation values. An attempt has been made to compare the experimental values with the results obtained using UDEC and other available model and check their effectiveness in predicting peak shear stress, peak shear displacement and peak dilation angle.

1.3 Organization of Report

- Chapter 1: Provides the introduction to the related field and deals about need of the work.
- Chapter 2: Describes the literature review of the topic in which various model for shear and dilation behaviour are discussed. Also various numerical techniques has been discussed which are available in order to simulate rock-joint behaviour.

- Chapter 3: Deals about the various joint properties needed for determination of shear strength and dilation and briefly discuss these terms and their significance in rock mechanics field.
- Chapter 4: Discuss about various test and their results performed in order to characterize the material and to study shear and dilation behaviour of rock joints.
- Chapter 5: In this chapter a brief introduction to UDEC tool has been given and modeling of joint and its results has been discussed. Also a comparison of results obtained by UDEC modeling and experimentation has been done.
- Chapter 6: This chapter sum up the various inferences made up during this study.
- Chapter 7: Scope of this project and future perspective has been discussed in this chapter.
- References: Here an account of several research publications has been made which were referred during this study.

CHAPTER 2

LITERATURE REVIEW

2.1 Shear Behaviour of Rock Joint

A natural discontinuity surface in rock is never as smooth and undulations and asperities are always present in the rock on a natural joint surface. These undulation and asperities have a significant influence on the shear behaviour of the joint and generally increases the shear strength of the surface. Compared to intact rocks jointed or fractured rock mass shows high permeability, higher deformation characteristics and low shear strength along the plane of discontinuity. Thus the study of strength parameters becomes very important for the analysis of effect of joints on rock mass. In case of rough joint surfaces shear displacement is accompanied by vertical displacement.

2.1.1 Patton Shear Strength Criteria, 1966

Patton in 1966 demonstrated the influence of roughness by means of shear test carried out on 'saw-tooth' specimens. According to Patton shear strength of saw-tooth specimens is represented by:

$$\tau_p = \sigma_n \tan(\Phi_b + i) \text{ For low normal stress} \quad (1)$$

$$\tau_p = c_0 + \sigma_n \tan(\Phi_b) \text{ For high normal stress} \quad (2)$$

Where, Φ_b is the basic frictional angle, i is initial asperity angle, c_0 is cohesion intercept.

2.1.2 Ladanyi and Archambault Shear Strength Criteria, 1970

$$\tau_p = \frac{\sigma_n(\nu+\tan\emptyset_b)(1-a_s)(a_s s_r)}{1-(1-a_s)\nu\tan\emptyset_b} \quad (3)$$

Where, a_s and ν are the proportion of total joint area sheared through the asperities and the rate of

dilatancy at the peak shear strength respectively and s_r is the shear strength of the rock comprising the asperities. Both a_s and ν are dependent on normal stress and are given by following relationship:

$$a_s = 1 - \left(1 - \frac{\sigma_n}{\sigma_T}\right)^{k1} \quad (4)$$

&

$$\nu = 1 - \left(1 - \frac{\sigma_n}{\sigma_T}\right)^{k2} \tan i_0 \quad (5)$$

Where, k_1 and k_2 are empirical constants with suggested values of 1.5 and 4, respectively and σ_T is the transitional stress.

Saeb and Amadei, 1992 modify Ladanyi and Archambault criteria. Their criterion led emphasis on the simultaneous contribution of shearing and sliding to the shear strength of a rock joint. In above equation a_s is the proportion of joint surface area sheared through the asperities and (1-a_s) is the proportion on which sliding occurs. The relative contribution of shearing and sliding depends on the of normal stress and generally at low normal stresses it has been observed that sliding is dominant while at high normal stresses asperity shearing is dominant.

2.1.3 Barton's Shear Strength Criteria, 1973

Patton's equation is valid at low normal stresses where shear displacement is due to sliding along the inclined surfaces while at higher normal stresses, the strength of the material get be exceeded and the teeth tend to break off which results in shear strength behaviour which is more closely related to the intact material strength than to the frictional characteristics of the surfaces. Barton 1973, 1976 studied the behaviour of natural rock joints and proposed the Patton's equation in new form:

$$\tau = \sigma_n \tan\{\Phi_b + JRC \log_{10}(\frac{JCS}{\sigma_n})\} \quad (6)$$

Where, JRC is joint roughness coefficient and ranges from 0-20

JCS is joint compressive strength and depends on σ_c

Barton and Choubey, 1977 revised their criteria for weathered rock joint by introducing the concept of residual strength. According to him:

$$\tau = \sigma_n \tan\{\Phi_r + JRC \log_{10}(\frac{JCS}{\sigma_n})\} \quad (7)$$

Where, Φ_r is residual friction angle and can be estimated from:

$$\Phi_r=(\Phi_b-20)+20(r/R) \quad (8)$$

where r is the Schmidt rebound number on wet and weathered fracture surfaces and *R* is the Schmidt rebound number on dry unweathered surfaces. The above equations have become part of the Barton-Bandis criterion for rock joint strength and deformability (Barton and Bandis, 1990).

2.2 Dilation Behaviour of Rocks

2.2.1 Introduction

Dilation (δ_v) is the relative moment between two joint faces along the profiles. In direct shear test, dilation is the movement of one surface with respect to other surface during shearing. In this study dilation is only the vertical displacement and hence should not be misinterpreted with the volumetric strain (ε_v) which is also referred as dilation in triaxial test.

Dilation can be represented in form of dilation angle as follows:

$$\tan d^\circ = \frac{\delta_v}{\delta_h} \quad (9)$$

Where d◦ is the dilation angle, δ_v is vertical displacement and δ_h is horizontal or shear displacement in mm.

Barton and Choubey, 1977 used peak secant dilation angle and tangent dilation angle for their studies.

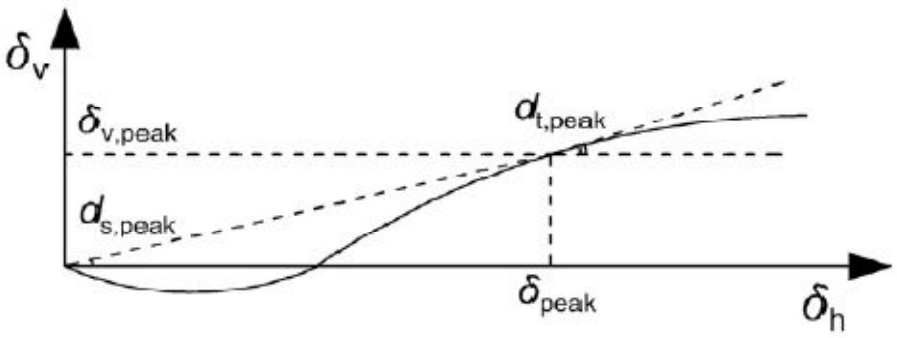

Figure 1.1: Typical shear displacement vs. dilation curve

From the above figure peak secant dilation angle (also known as initial dilation angle) $d_{s,peak}$ can be best represented by:

$$d_{s.peak} = \tan^{-1}\left(\frac{\delta_{v.peak}}{\delta_{peak}}\right) \tag{10}$$

And peak tangent dilation angle $d_{t,peak}$ represented by:

$$d_{t.peak} = \left(\frac{\partial \delta_v}{\partial \delta_h}\right)_{at\,\delta_h = \delta_{peak}} \tag{11}$$

Where $\delta_{v.peak}$ is dilation corresponding to δ_{peak} and δ_{peak} is shear displacement corresponding to peak shear stress (τ_p).

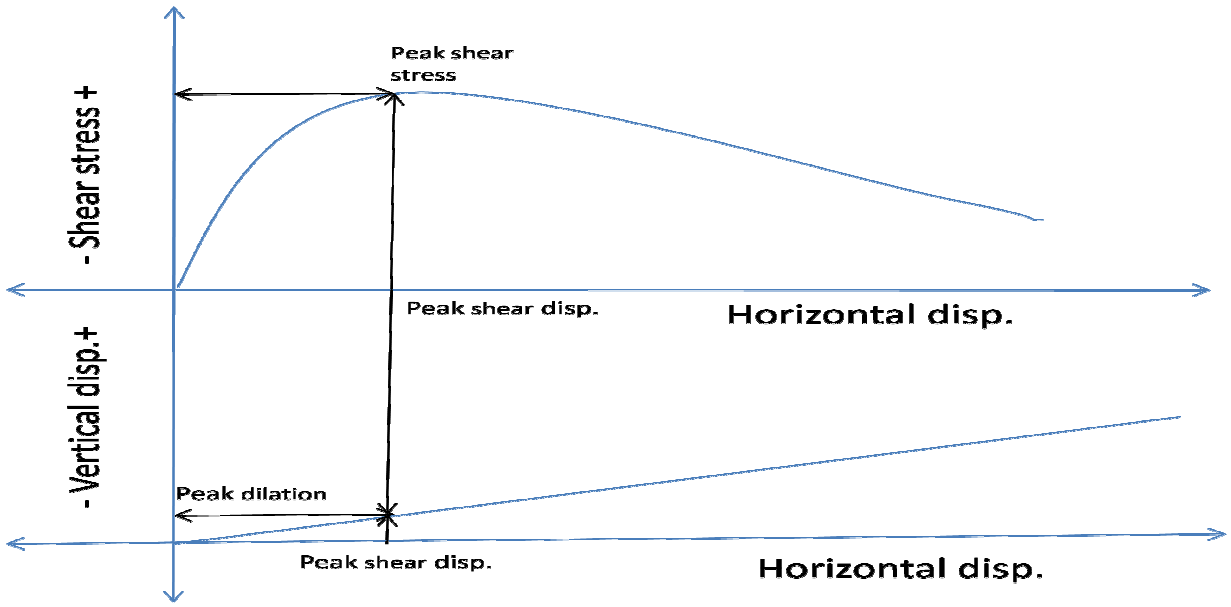

Figure 1.2: Typical result of Direct Shear Test

2.2.2 Model of Ladayani and Archambault, 1970

Ladayani and Archambault, 1970 proposed the following relation to determine peak tangent dilatancy :

$$\tan i_p = \left(1 - \frac{\sigma_n}{\sigma_T}\right)^{k_2} \tan i_{po} \qquad (12)$$

Where, k_2 is an empirical coefficient influenced by joint surface roughness and having values in range between 0.25 and 3.55; σ_T is a transitional stress beyond which no further dilatancy takes place; $\tan(i_{po})$ is the peak rate of dilatancy at zero normal stress.

2.2.3 Barton and Choubey, 1977

They explained following points:

1) Both peak and initial dilation angles were occasionally negative or zero. In such cases the joints did not start to dilate significantly until after peak strength was reached, and in fact may

have contracted. When this type of dilation occurs in spite of a quite high asperity component, it signifies that the joint "failed" when a small steep interlocking projection failed.

2) They found that peak secant dilation angle is equal to the difference between the measured total friction angle ($\tan^{-1}\tau_p/\sigma_n$) and the estimated residual friction angle (Φ_r) and they also showed that peak secant angle is about one-third of the peak tangent dilation angle.

3) Majority of peak dilation angle fall between the range:

$$0.5\ JRC\ \log_{10}(JCS/\sigma_n) < d_{t.peak} < 2\ JRC\ \log_{10}(JCS/\sigma_n) \tag{13}$$

4) They give the following relationship to estimate the peak secant and tangent dilation angles

$$d_{t.peak} = JRC.\log_{10}\left(JCS/\sigma_n\right) \tag{14}$$

$$d_{s.peak} = \frac{1}{3}JRC.\log_{10}\left(JCS/\sigma_n\right) \tag{15}$$

5) They then introduce the factor 'M' known as damage coefficient such that:

$$M = \frac{JRC}{12.\log_{10}(JCS/\sigma_n)} + .70 \tag{16}$$

Value of M can also be taken as 1 or 2 for shearing under low or high stress respectively (Olsson and Barton, 2001). The value of peak tangent dilation angle can then be corrected by dividing it by the factor M.

Barton, 1982 state that dilation will begin when $JRC_{mobilized}=0$ and in that case mobilized tangent dilation angle, d_t can be estimated from the following relationship:

$$d_{t.mobilized} = \frac{1}{M}JRC_{mobilized}.log_{10}\left(JCS/\sigma_n\right) \tag{17}$$

where,

$$JRC_{mobilized(\delta_h)} = \frac{\tan^{-1}(\tau(\delta_h)/\sigma_n) - \emptyset_r}{\log(JCS/\sigma_n)} \tag{18}$$

Asadollahi, 2010 also give an equation for the calculation peak secant dilation angle by performing regression analysis on 341 direct shear test result and equation are:

$$d_{s.peak} = \tan^{-1}\left(\frac{1}{3}\tan\left(JRC.\log\left(\frac{JCS}{\sigma_n}\right)\right)\right) \quad (19)$$

He also proposed an emphirical model for pre-peak dilatancy behaviour of rock fractures and dilation displacement can be calculated at each shear displacement using this equation. Also this model does not contain any of the inconsistancies and ambiguity of Barton's model:

$$\frac{\delta_v}{\delta_{peak}} = \frac{1}{3}\tan\left(JRC.\log\left(\frac{JCS}{\sigma_n}\right)\right).\left(\frac{\delta_h}{\delta_{peak}}\right).\left\{2\left(\frac{\delta_h}{\delta_{peak}}\right) - 1\right\} \quad (20)$$

2.3 Peak Shear Displacement in Rocks

It has been explained earlier that peak shear displacement is the horizontal displacement required to reach peak shear strength. Bandis et. al., 1981 indicated that δ_{peak} is generally about 1% of the joint sample length (L). For example in case of laboratory-size samples (L_0 = 100 mm), during shearing first 1 mm of shear displacement Φ_r is mobilized first, and then roughness, causing post-peak dilation, at displacements larger than our example 1mm, roughness is gradually destroyed or work down and dilation continues but at a reduced rate post-peak.

Bandis et. al, 1981 give an empirical relationship to estimate δ_{peak} from the analysis of 650 shear test. He found that δ_{peak} is dependent on the sample length (L in meters) and the roughness JRC of the sample:

$$\frac{\delta_{peak}}{L} = \frac{1}{500}\left(\frac{JRC}{L}\right)^{.33} \quad (21)$$

L and δ_{peak} are in metrers

Barton in 1982 relates the ratio of $JRC_{peak}/JRC_{mobilized}$ with the ratio of δ_h/δ_{peak}:

Table 1: Recommended model for shear stress–displacement (Barton, 1982)

Non-planar fractures		Planar fractures (JRC≤5)	
δ_h/δ_{peak}	$JRC_{mobilized}/JRC_{peak}$	δ_h/δ_{peak}	$JRC_{mobilized}/JRC_{peak}$
0	$-\Phi_r/i$	0	$-\Phi_r/i$
0.3	0	0.3	0
0.6	0.75	0.6	0.75
1.0	1.0	1.0	0.95
2.0	0.85	2.0	1.0
4.0	0.70	4.0	0.9
10.0	0.50	10.0	0.7
25.0	0.40	25.0	0.5
100	0	100	0

Asadollahi, 2010 proposed an equation for the prediction of peak shear displacement based on the regression analysis of about 317 samples. Equation has been found good in predicting peak shear displacement compared to the Barton's equation. The equations are for joints:

$$\delta_{peak} = .007L^{.45}\left(\frac{\sigma_n}{JCS}\right)^{.34}\cos\left(JRC\log\left(\frac{JCS}{\sigma_n}\right)\right) \quad (22)$$

where, L is length of the block is in meters and δ_{peak} is also in meters

2.4. Numerical Methods in Rock Engineering

Numerical method can be broadly classified into three methods: continuum method, discontinuum method and hybrid method (Jing and Hudson, 2002).

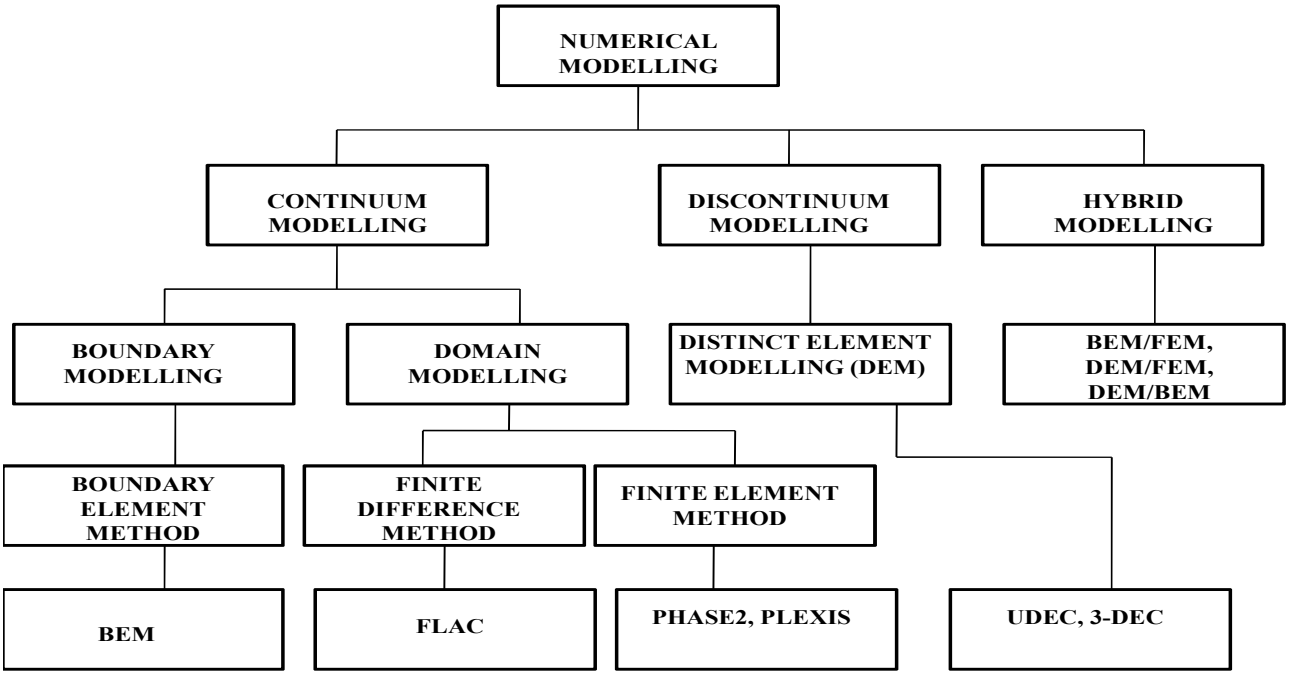

Figure 2.3: Different Methods of Numerical Modelling

In continuum method rock mass is treated as a continuous material. In this method the problem domain is divided into finite number of elements and than their behaviour is approximated by simpler mathematical equations. These elements must satisfy governing equations and compatibility condition at interfaces with adjacent elements (L. Jing, 2003; Jing and Hudson, 2002). In the continuum approach plastic softening and damage models are most common techniques for capturing failure and localization (De Borst, 2002). The most commonly applied methods based on continuum approach are finite element method (FEM), finite difference method (FDM), boundary element method (BEM)

In discontinuum method Rock is represented as a discontinuous mass. Blocky nature of system is analyzed and it is assumed that block may interact with neighboring block through the joints and special emphasis is devoted for the characterization of rock element, rock joint and

discontinuities (Barla et.al, 1999). The most important methods based on this approach are distinct element method and discrete fracture nature method (DFN).

Continuum methods may include the discontinuities in the medium if present, explicitly or implicitly, while in discontinuum methods discontinuities are included explicitly (Bobet.et.al, 2011). There is no quantitative guideline for the suitability of one method over other. The choice of continuum or discontinuum method depends on highly on the problem scale and fracture system of geometry. Brady 1987 provides some qualitative guidance. In general the continuum approach can be used if only few fractures are present and complete block detachment are not significant factors and discontinuum approach is suitable for moderately fractured rock masses or where large-scale displacement of individual blocks are possible (Jing, 2003). A pseudo-continuous displacement field is assumed to be formed if medium is heavily jointed such that the blocks defined by discontinuities have a size much smaller than the opening, and in such cases use of continuum model seems reasonable (Bobet.et.al, 2009).

The disadvantage of each method can be avoided by combined continuum and discontinuum models. Basic approach is to model far-field as isotropic continuum using BEM and the near-field fractured rock by using either DEM or FEM and combinations are FEM/BEM, BEM/DEM, and FEM/DEM.

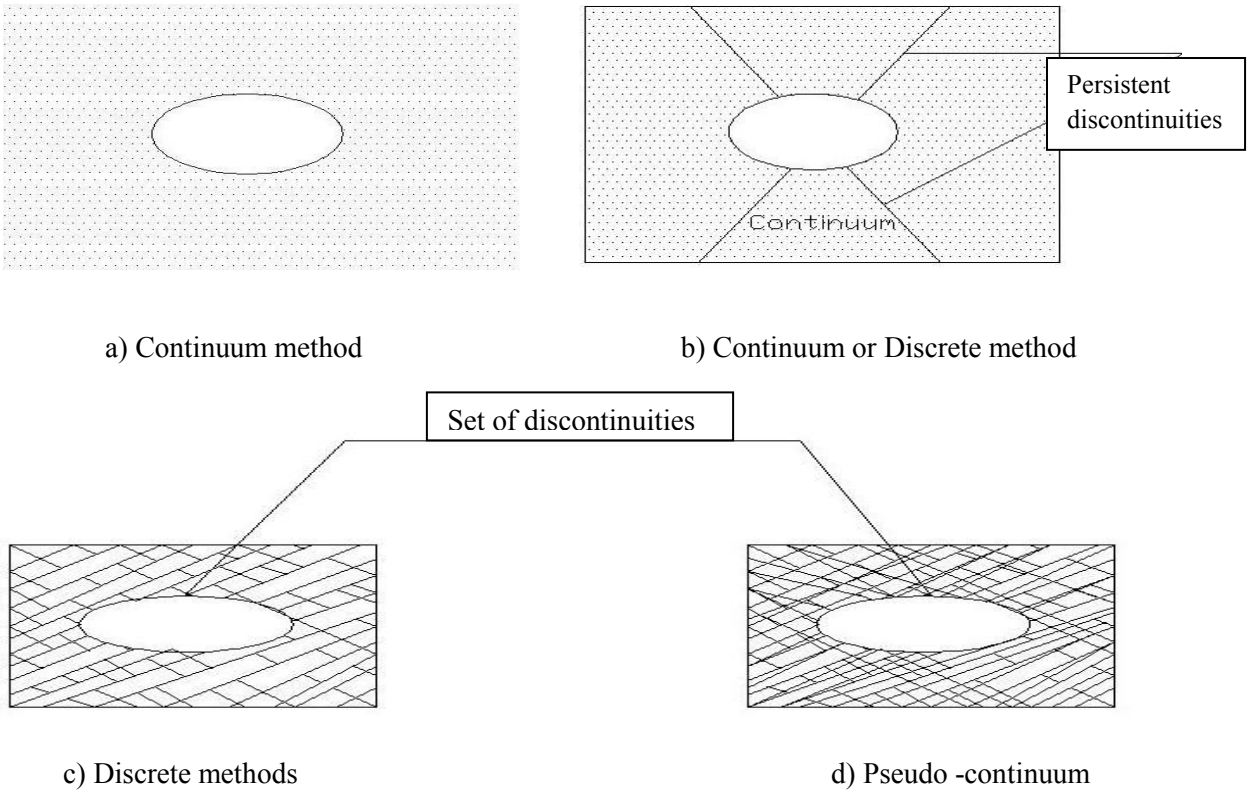

Figure 2.4: Suitability of different methods for an excavation in a rock mass

(Jing, 2003 and Bobet.et.al, 2009)

2.4.1. The FDM and Related Methods

The basic technique in the FDM is discretization of the governing PDE's by replacing the partial derivative with the differences at neighboring gird points. The solutions for the system equation are obtained by imposing necessary initial and boundary conditions. The continuum is represented by a series of discrete grid point at which displacements, velocities and accelerations are calculated. The displacement field is computed by approximating the differential equations for the system as a set of difference equations (central, forward or backward) that are solved discretely at each grid point. The differential equations are approximated through the use of difference equations (Jing and Hudson, 2002; Jing, 2003)

Grid system is a convenient way generating objective functional values at sampling points with small interval between them, so that errors incurred will be small and acceptable. The formation and solutions of the equations are localized, which is more efficient for storage handling in computer implementation. It is the most direct and interactive technique for the solutions of PDE's and also provides the additional advantage of direct simulation of complex material, such as damage and plasticity.

According to Perrone and Kao, 1975, Beer and Watson, 1992 in FDM irregular meshes, such as quadrilateral gird are generated and these grids enhance the applicability of the FDM for rock mechanics problems. This approach is so called Finite volume method. For unstructured grid, the FVM is formulated at nodes (grid points) or at the center of the elements with the help of displacement variable. It has similarities with the FEM and act as a bridge between the FDM and FEM.

The most well known computer code using for stress analysis for rock engineering problems using the FVM/FDM approach is the FLAC code group (ITASCA Consulting Group, Inc. FLAC Manual). Representation of fractures is not easy in the FDM/FVM because they require the continuity of the grid points. On the other hand, FDM/FVM models have been used to study the mechanisms of fracturing processes, such as shear formation in the lab testing of rock and soil samples. The FVM is one of the most popular methods in rock engineering, covering all aspects which are related to Rock mechanics such as Slope stability, underground openings, and hydro mechanical or thermal hydro mechanical process.

2.4.2. The FEM and Related Methods

In FEM domain discretization involves dividing the domain into the number of sub domain of standard shapes (triangular, tetrahedral and quadrilateral) with fix number of nodes at vertices and / or on the sides. Polynomial functions are generally used as trial functions in order to approximate the behavior of PDE at element level and by generating local algebraic equations for representing the behavior of elements. The elements equations are categorized according to the topological relation between nodes and elements and then assembled in to global system of algebraic equation, the solution that provides the required information in the solutions domain. As this model is based on continuum assumptions, block rotation, sliding, large scale opening and complete detachment are not permitted and formulation of FEM requires that fractured or jointed elements cannot be torn apart (Jing, 2002).

Due to its flexible approaches in handling material heterogeneity and anisotropy, complex boundary conditions and dynamics problems makes FEM, one of the best popular numerical method. In order to counter the material in homogeneity in FEM different materials properties are assigned to different elements. In order to consider the effect of an infinite far-field domain on the near –field behaviour 'infinite domain element" has been developed in FEM (Beer and Meck, 1981). Many computer codes has been generated based on FEM of which PLAXIS, PHASE-2, and ABQUAS are most popular.

Treatment of fractures and fracture growth is the most important factor which limits the application of FEM in rock mechanics. Requirement of small element size, continuous re-meshing with fractures and conformable fracture path and elements edge for simulating the fracture growth process make FEM inefficient in dealing with such fractured rock mass problem.

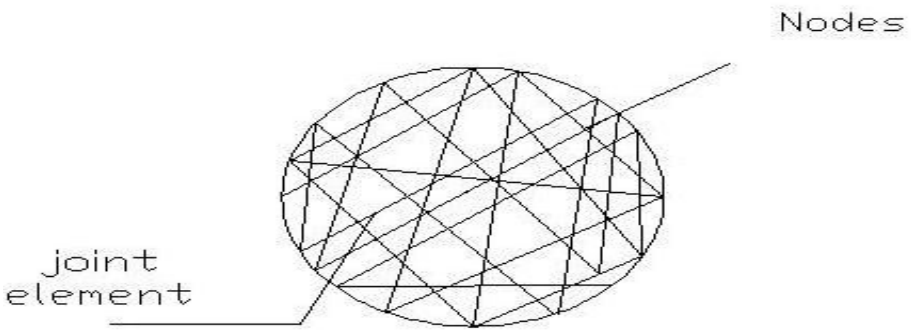

Figure 2.5: Representation of a fractured rock mass by FEM.

2.4.3. The BEM and Methods

Initially BEM approach seeks a weak solution of an integral equation which is derived using Betti's Reciprocal theorem. The introduction of isoperimetric elements using different orders of shapes function greatly enhanced the BEM's applicability for stress analysis problems.

This method derives its name from the fact that the user 'discretizes', or divides into elements, only boundaries of the problem geometry (i.e., excavation surfaces, the free surface for shallow problems, joint surfaces and material interfaces), thus reducing the problem dimensions by one and greatly simplifying the input requirements. In this method the conditions on a surface could be related to the state at all points throughout the remaining medium, even to infinity. The information required in the solution domain is separately calculated from the information on the boundary, which is obtained by solution of boundary integral equation.

In order to simulate the fracture growth using BEM, two techniques are used. First is to divide the problem domain into multiple sub domains with fractures along with their interfaces, with a pre-assumed fracture path. Second is the dual boundary element method (DBEM) using displacement and traction boundary equations at opposite surfaces of fracture elements (Jing,

2003). Galerkin BEM or GBEM is the special case of BEM, which produces a symmetric coefficient matrix which is solved by double integral formulation.

Input data preparation is comparatively is generally simpler in case of BEM as simpler mesh are generated with decreased model reduction. But BEM is not as efficient as FEM in dealing material heterogeneity as it does not contain many sub-domains as contained by an element in FEM. BEM is also not efficient for simulating non-linear material behaviour. According to Jing and Hudson, BEM has been found more suitable in case of problems related to fracturing of inhomogeneous and linearly elastic bodies, stress and deformation analysis for underground excavations, soil-structure interaction, groundwater flow and fracturing processes and some of its uses are as: i) Structure analysis of underground excavations with and without fracture; ii) Dynamic Analysis; iii) Elastic properties; iv) Borehole tests for permeability measurements.

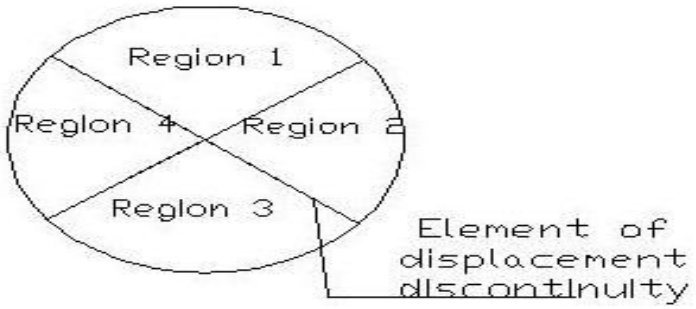

Figure 2.6: Representation of a fractured rock mass by BEM.

2.4.4. The DEM and Related Methods

DEM is a lagrangian numerical technique where the computational domain consists of discrete solid elements that interact via compliant contacts (Bobet et.al, 2009*)*. Basic concept of DEM is that the domain of interest is generally treated as an assemblage of rigid or deformable blocks

and contact information among each block is identified and updated continuously during the deformation process.

The theoretical foundation of the method is to derive and solve the equation of motion of rigid and/or deformable blocks using implicit (based on FEM discretization) and explicit (based on FDM/FVM discretization) formulation. It has been assumed in DEM that discontinuities divide the medium and bound finite number of blocks through their intersection. These blocks are in turn interconnected through the discontinuities.

Three main issues which are needed to be addressed by DEM are (Cudall and Hart, 1992; Jing, 2003):

1. Representation of contacts i.e. identification of blocks or particle system based on the fracture geometry or on the particle shape assumption within the domain.
2. Formulation and solution of equation of motion representing the behavior of particle system.
3. Detecting and continuously updating the contact information during the execution of discrete system.

The main difference between DEM and continuum based methods is that the contact pattern is fixed in continuum approach while continuously changing and updating in DEM. The explicit representation of fractures makes DEM, most attractive and suitable method for rock mass modeling. Many explicit computer codes has been developed based on DEM approach, UDEC and 3-DEC are two such computer codes for two and three dimensional problems in rock mechanics (ITASCA Consulting Group).

Though DEM as is flexible and powerful tool for analyzing discontinuous rock but difficulty associated in obtaining reliable data on location, orientation and persistence of discontinuities, lack of information on material behaviour limits its application. But in general it remains as qualitative and useful tool for deformation analysis of fractured blocky rock mass and also provides an insight into failure mechanism.

Discontinuous deformation analysis (DDA) is the method of representing implicit DEM. It was first formulated by Shi and Goodman, 1984, 1985 and was further developed for stress-deformation analysis, and for coupled stress-flow problem. According to Jing and Hudson, 2002 and Jing, 2003 DDA method uses standard FEM meshes over blocks and contacts are treated using penalty method. According to Shi, 1988 medium is discretizes into elements or blocks that are in contacts with each other only through their boundaries

DDA has two main advantages over explicit DEM:

1. Relatively larger time steps and closed-form integration for stiffness matrices of elements.

2. An existing FEM code can also be readily transformed into a DDA code while retaining all advantageous features of FEM.

Discrete Fracture Network (DFN**)** method is a special discrete model which was created in early 1880s for both two and three dimensional problems. DFN model considers fluid flow and transport processes in fractured rock masses through a system of connected fractures flow. Its application is found for the study of flow in fractured media, for the derivation equivalent continuum and transport properties of rock The basis of DFN model is the knowledge, understanding and representation of fracture system geometry and transmissivity of individual

fractures (Jing. 2002), hence like in DEM, stochastic simulation of fracture system also plays an important role in the performance and reliability of DFN model. Due its conceptual attractiveness it has find many application for modeling of fractured rock mass problem. The main computers codes based on DFN approach are FRACMAN/MAFIC and NAPSAC.

It is difficult to model the effects of mechanical deformation and heat transfer on fluid flow in DFN also lack of knowledge of geometry of rock fractures limits its application.

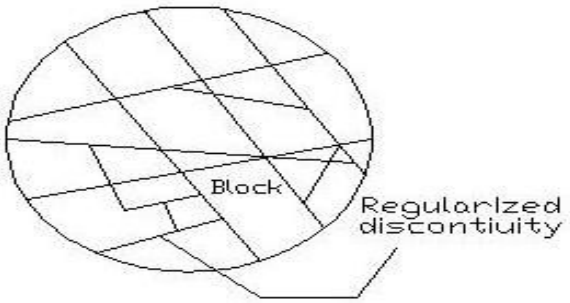

Figure 2.7: Representation of a fractured rock mass by DEM.

2.4.5. Hybrid Models and Related Methods

It is the approach comprising the combination of both Continuum and discontinuum methods such that disadvantage of each method are avoided .The main types of hybrid models are FEM/BEM, BEM/DEM and FEM.DEM. Generally it is assumed that far-field rock act as an equivalent elastic continuum, and near-field is assumed as fractured and non-linear in behaviour hence requires explicit representation of fractures. Commonly BEM is used for simulating far-field and FEM and DEM is used for near-field. Hybrid models are being frequently used in rock engineering for flow and stress/deformation problem (Jing, 2003)

Hybrid FEM/BEM models method was presented as a stress analysis technique by Brady and Wassyng, 1981 and Beer, 1983. It has found its application for simulating the mechanical behaviour of underground excavations.

Hybrid DEM/BEM models was implemented only for the explicit DEM, referred to the code group of UDEC and 3DEC. It is technique which is created by Lorig and Brady 1982, 1984, 1986. The basic concept is to treat the far-field BEM region as a super block region having contacts with smaller blocks along the interfaces with near-field DEM region.

Hybrid DEM/FEM models is the one in which the DEM region consists of rigid blocks and FEM region consists of material having non-linear behaviour. Though hybrid models are very useful, special attention needed for continuity or compatibility condition at the interfaces between regions of different model (Jing, 2003).

CHAPTER 3

ROCK JOINT PROPERTIES

3.1 Uniaxial Compressive Strength (UCS)

Unconfined compressive strength of rock can be determined from Schmidt Hammer Test, Point Load Test and Unconfined Compression Test.

The Schmidt Hammer is a simple device for recording the rebound of a spring loaded plunger after its impact with a surface. The L-hammer used generally for experimental study (impact energy =0.075 m.kg) is suitable for testing small and impact-sensitive parts of concrete and artificial rocks. It is suitable for measuring UCS values of about 20N/mm^2 to 300N/mm^2

Miller, 1965 gives a empirical equation for rebound number ranging from 10 to 100 and uniaxial compressive strength (σ_c) of rock.

$$\log_{10} \sigma_c = .0088\gamma R + 1.01 \tag{23}$$

Where, σ_c= uniaxial compressive strength of surface in N/mm^2; γ =dry density of rock (kN/m^2) and R= rebound number.

Uniaxial compressive strength of a rock sample can also be calculated form Point Load Strength as suggested by ISRM (1985). The point load index is defined as:

$$I_s = \frac{P}{D_e^2} \tag{24}$$

where, D_e is the equivalent core diameter in mm

For non-circular cross-sections$D_e = \sqrt{\frac{4A}{\Pi}}$, in which A is the minimum cross-sectional area of a plane trough the specimen.(Asadollahi et.al, 2010). The values I_s, should be modified for diameter corrections:

$$I_{(s)50}=F \times I_{(S)} \quad (25)$$

and $$F=(D_e/50)^{0.45} \quad (26)$$

ISRM suggest that uniaxial compressive strength is about 20-25 times of point load index.

The uniaxial compression test measures the unconfined compressive strength, Young's modulus, and poisson ratio of rock material (Brady and Brown, 2004).

3.2 Joint Wall Compression Strength (JCS)

According to Barton, measurement of JCS is of fundamental important since it is largely the thin layers of rock adjacent to joint walls that control the strength and deformation properties of the rock mass as a whole. The value of JCS varies according to the weathering condition of joints. The depth of penetration of weathering into joint walls invariably depends on rock type and permeability of rock.

The weathering process of a rock mass can be summarized in the following simplified stages (Barton and Choubey, 1976):

1) Formation of joint in intact rock: JCS value same as σ_c since no weathering.

2) Slow reduction of joint wall strength if joints are water-conducting: JCS<σ_c.

3) Intermediate stage; weathered, water conducting joints, impermeable rock blocks between, JCS some fraction of σ_c.

4) Penetration of joint weathering effect into rock blocks; progressive reduction of σ_c from the walls of the blocks inwards, JCS continues to reduce slowly.

5) Advanced stage of weathering; more uniformly reduced σ_c finally drops to same level as JCS, rock mass permeable throughout.

In general if no direct measurement are available (Barton, 1973):

For unweathered joint: JCS= σ_c

For weathered joint: JCS= σ_c /4

3.3 Joint Roughness Coefficient (JRC)

Surface roughness of joint plane can also be quantified using a Joint Roughness Coefficient Index (JRC) introduced by Barton and Choubey, 1976. The JRC varies between 0 and 20 and is obtained by comparing the discontinuity roughness profile to a series of reference profiles given by Barton and Choubey, 1977.

JRC can also be estimated by Tilt test on rough surface with Schmidt hammer index test, and Tilt test on saw tooth rock surface. This is an indirect method in order to estimate the JRC:

$$JRC = \frac{\propto^{\circ} - \emptyset_r}{\log_{10}\frac{JCS}{\sigma_{n0}}} \tag{27}$$

where, α° is the tilt angle, Φ_r is the residual friction angle, σ_{no} is the normal stress acting on joint at tilt failure.

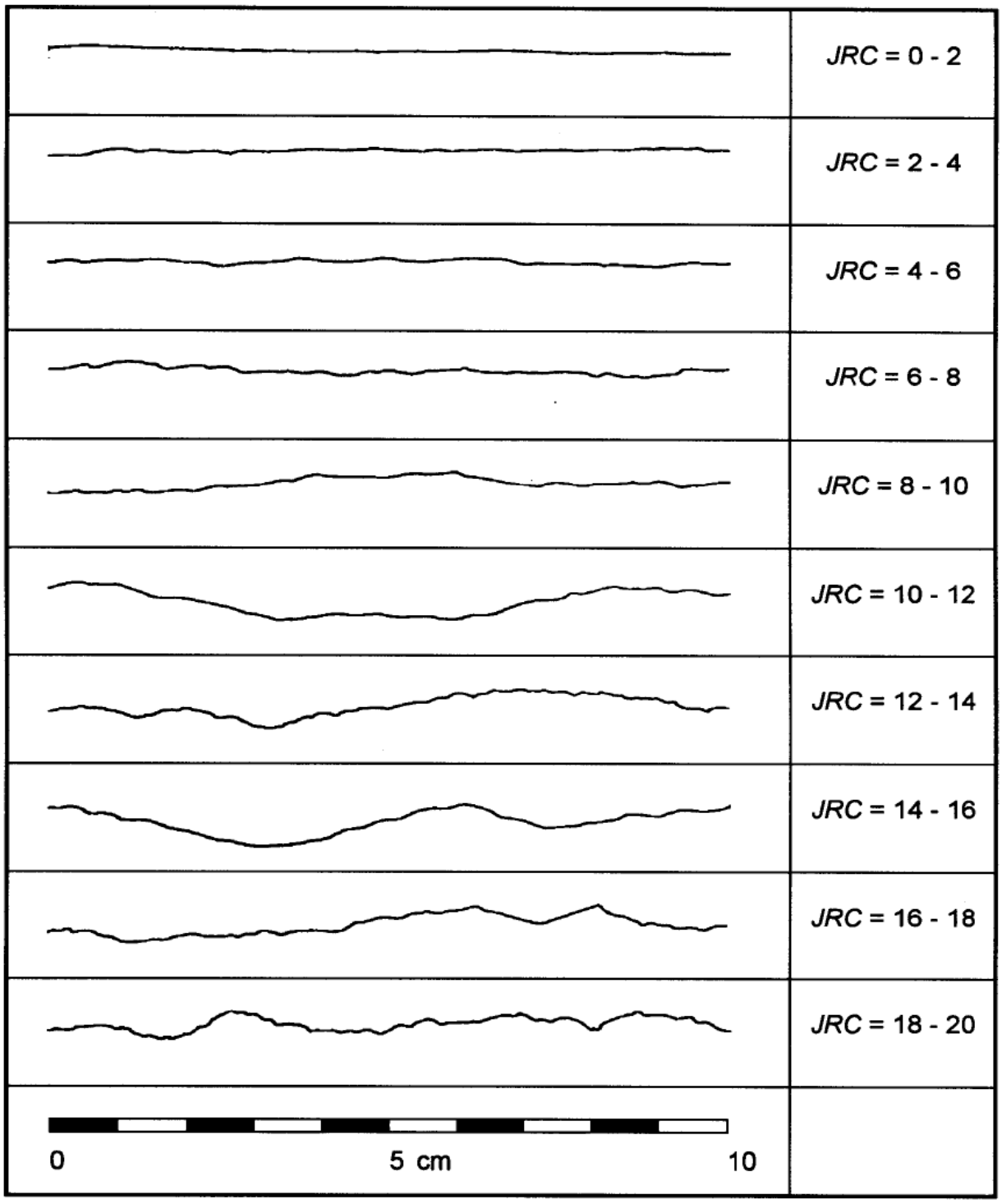

Figure 3.1: Roughness profile (Barton and Choubey, 1977)

In the year 1979, Tse and Cruden, 1979 and Xie and Paariseau, 1992 suggested a method based on the geometrical dimension for tooth shaped asperities:

Tse and Cruden, 1979: $JRC=32.2+32.47 \log_{10} Z_2$ (29)

$$Z_2 = \left[\frac{1}{L}\int_{x=0}^{x=L}\left(\frac{dy}{dx}\right)^2 dx\right]^{1/2} \quad (30)$$

where, y is the amplitude roughness about centerline, dx is the small constant distance between two adjacent amplitude readings.

Xie & Pariseau, 1992: $JRC=85.27(D-1)^{0.57}$ (31)

$$D = \frac{\log(4)}{\log\left[2\left(1+\cos\tan^{-1}\left(\frac{2h}{L}\right)\right)\right]} \quad (32)$$

where, JRC, D, h, and l are joint roughness coefficient, fractal dimension, average asperity height, and average asperity base length, respectively.

Maksimovic, 1996: $JRC= i_0/2$ (33)

where i_0 is initial asperity angle

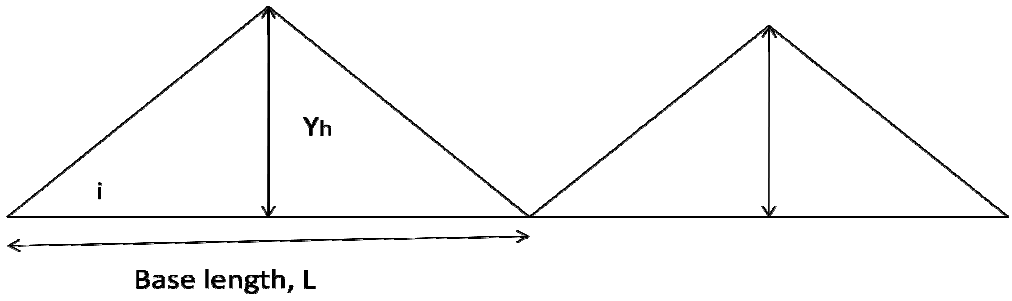

Figure 3.2: Geometry of Asperities

3.4 Scale Effect on JRC and JCS

After reviewing various literatures and conducting appreciable amount of testing of joints, joint replicas, Barton and Bandis, 1982 proposed the scale corrections for JRC and JCS defined by the following relationship:

$$JRC_n = JRC_0 \left[\frac{L_n}{L_0}\right]^{-.02JRC_0} \quad (34)$$

and

$$JCS_n = JCS_0 \left[\frac{L_n}{L_0}\right]^{-.03JCS_0} \quad (35)$$

where JRC_o, JCS_o , L_o (length) refer to 100 mm laboratory scale samples and JRC_n, JCS_n and L_n refer to in situ block sizes. There is a greater possibility of weaknesses in a large surface, and average joint wall compressive strength (JCS) may decreases with increasing scale (Barton and Bandis, 1982)

3.5 Joint Stiffness Characteristic

Joint stiffness parameters describe the stress-deformation relationship of the joint. They are fundamental properties of rock joint and extremely important in the numerical modelling of jointed rock. Joint shear stiffness and joint normal stiffness are being discussed below:

3.5.1 Joint Shear Stiffness (K_s)

Joint Shear Stiffness is defined as the average gradient of the shear stress-shear displacement curve for the section of the curve below peak strength Barton, 1972. It can be measured from the result of direct shear test and its value varies with, size of the sample tested and also increases with an increase in normal stress (Bandis et al. 1983).

Barton and Choubey, 1977 suggested the following equation for the estimation of the peak

shear stiffness (MPa/m):

$$k_s = \frac{100}{L_x}\sigma_n \tan\left\{\text{JRC}\log_{10}\left(\frac{\text{JCS}}{\sigma_n}\right) + \emptyset_r\right\} \quad (36)$$

Where, L_x is the joint length in meter. This equation is based on the assumption that the peak shear strength is reached after the shearing of approximately 1% of the joint length.

3.5.2 Joint normal stiffness (K_n)

Joint normal stiffness is defined as as the normal stress per unit closure of the joint. Joint normal stiffness is influenced by the following factors (Bandis et al., 1983):

i) the initial actual contact area; ii) the joint wall roughness; iii) the strength and deformability of the asperities; and iv) the thickness, type and physical properties of any infill material.

Bandis et.al, 1983 suggested the following equation for the estimation of normal stiffness:

$$K_n = K_{ni}\left[1 - \frac{\sigma_n}{V_m K_{ni} + \sigma_n}\right]^{-2} \quad (37)$$

where, V_m is joint maximum closure;

K_{ni} is initial joint stiffness and can be obtained by:

$$K_{ni} = -7.15 + 1.75JRC + .02\left(\frac{JCS}{a_j}\right) \quad (38)$$

& a_j is initial joint aperture in mm under self weight such that:

$$a_j = \frac{JRC}{5}\left(0.2\frac{\sigma_c}{JCS} - 0.1\right) \quad (39)$$

CHAPTER 4

EXPERIMENTAL SETUP

4.1. Experimental Setup

Experimental program can be broadly divided into two parts: i) material characterization; ii) direct shear testing of rock joints.

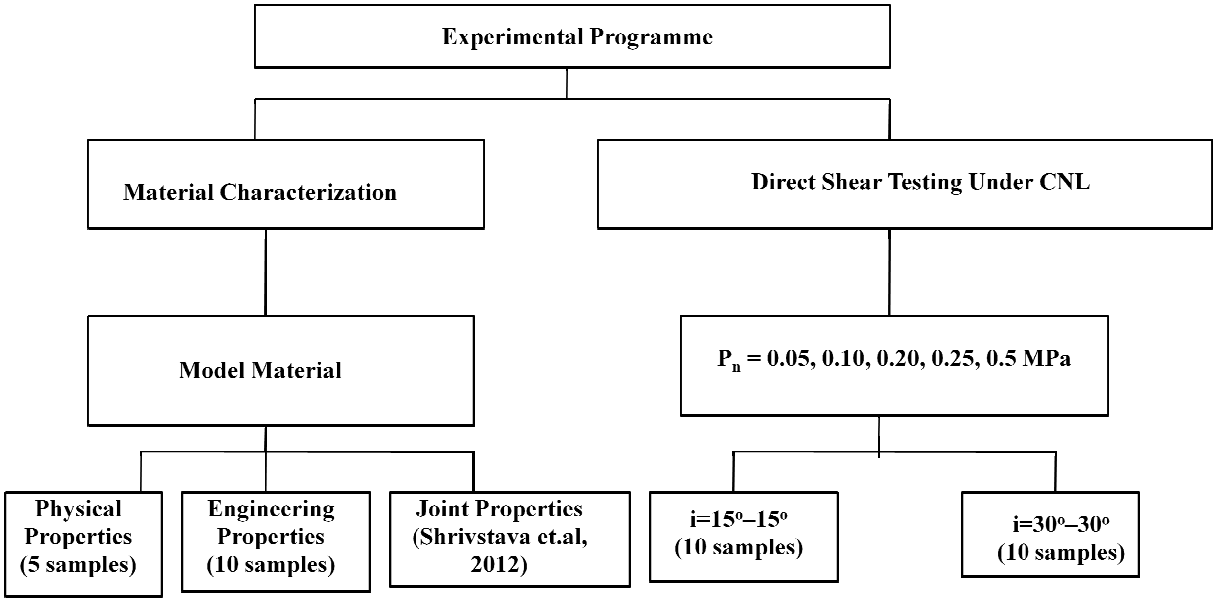

Figure 4.1: Flow Chart of Experimental Setup

For model material characterization properties of material are determined such as specific gravity, particle size distribution, setting time, unconfined compressive strength etc.

In direct shear testing firstly artificial jointed sample are modeled and then testing is done on samples in order study the behaviour. Both shear as well as dilation properties are studied in laboratory investigation.

4.1.1 Materials Used

It is very difficult to obtain the core of rock sample in field and conducting experiments on it, therefore behaviour of rock joints is simulated by molding artificial rock joints using some model material. Model material should such that uniform, identical and homogeneous joint specimen in order to understand the failure mechanism, deformation behaviour and strength of rock joints. It has been observed that Plaster of Paris is good for simulating weak rock mass. Many researchers

have used Plaster of Paris as model material because of its ease in casting, flexibility, setting, low cost and easy availability.

Plaster of Paris is a type of building material obtained from Gypsum plaster ($CaSO_4.0.5H_2O$ hemihydrates) by heating gypsum at a temperature of about 300◦F. It can be easily molded into any shape when mixed with water, and the long-term strength is independent of time once the chemical hydration is completed. It has been found suitable for simulating the behaviour of jointed soft rocks such as coal, friable limestone, clay shale and mudstone. In this study material characterization of Plaster of Paris has been done. Plaster of Paris of Trimurti Brand has been used for this study.

4.1.2. Preparation of Specimens

A bag (20 kg) of Plaster of Paris is brought from the local market. The Plaster of Paris is in powder form and is produced by pulverizing partially burnt gypsum which is duly white in color with smooth feel of cement. Initially, water content taken for study is 30%, 40%, and 50% by weight of Plaster. Initial and final setting time for each of this water content is determined and unconfined compression test are carried on intact samples prepared for the three water content is carried out after 7 days of air curing. After the analysis of test result and experience obtained during testing, it has been observed that though uniaxial compressive strength for 30% and 40% water content is higher than that of 50 % water content but initial setting and final setting time is low for them, also workable mixture is not obtained for them and molding of sample is difficult 30% and 40% compared to 50% water content. Hence 50% water content has been finally selected for sample preparation for further study. For preparation of specimen Plaster of Paris is mixed thoroughly with 50% (by weight) water to form a uniform paste. The Plaster of Paris

specimens are prepared by pouring the plaster in the mould and continuously tamping and shaking for approximately 2-3 min for proper compaction and to avoid presence of air gaps. After that it is allowed to set for 5 min and after hardening, the specimen was extruded manually from the mould and left for curing.

4.1.2.1 UCS Test

Sample for unconfined compressive test is prepared according IS 2720 Part 10-1991. UCS mould is hollow cylinder with length to diameter ratio greater than 2 (L/D>2). The standard length or height of the mold was 76mm and diameter was 38mm having cross-section area of 1134.1149 mm^2. Before starting sample preparation, standard mould is thoroughly oiled in inner surface so that sample can be extruded easily. For preparation of specimen, 150gm of Plaster of Paris is mixed thoroughly with 75ml (50% by weight) water to form a uniform paste. This paste is than poured in the standard mould with continuous shaking and tamping during pouring. After that it is allowed to set and after hardening, the specimen was extruded by opening the mould. The samples are than allowed dry out in air for 7 and 14 day.

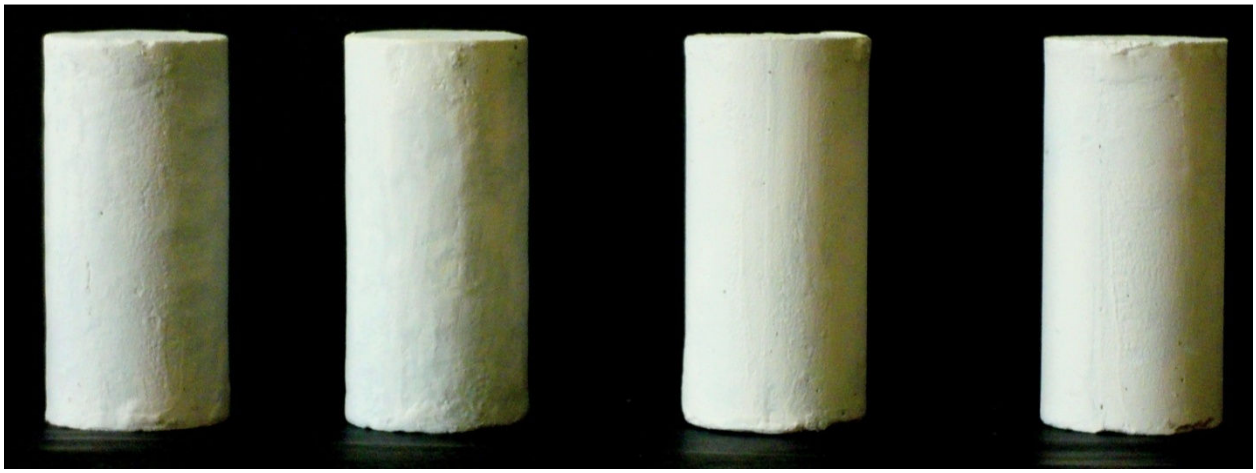

Figure 4.2: UCS Sample for Curing

4.1.2.2 Direct Shear Test

For preparation of samples for direct shear test two moulds of size 60mmx60mmx25mm are casted with mild steel. These moulds are provided with screw arrangement so that they can be easily opened using key. For making joints, two sheets made up of plastic of thickness approximately 1mm are molded in the form of continuous and uniform joint pattern with angle 30° and 15°. Inner surface of mould are oiled properly. Uniform paste of plaster is formed by adding 50% water by weight. During preparation of jointed sample firstly one block is casted with joint pattern sheet at the bottom. Once this sample block is fully set it is inverted with joint pattern sheet and oiling is done on the surface of sheet and other metal block is kept on their top and plaster paste is than poured in it with continuous shaking for better compaction and avoid air entrapping. After setting, arrangement is removed and mould are opened using alenkey, and sample from upper and lower mould are taken our carefully. Then sample are left for curing for 14 days.

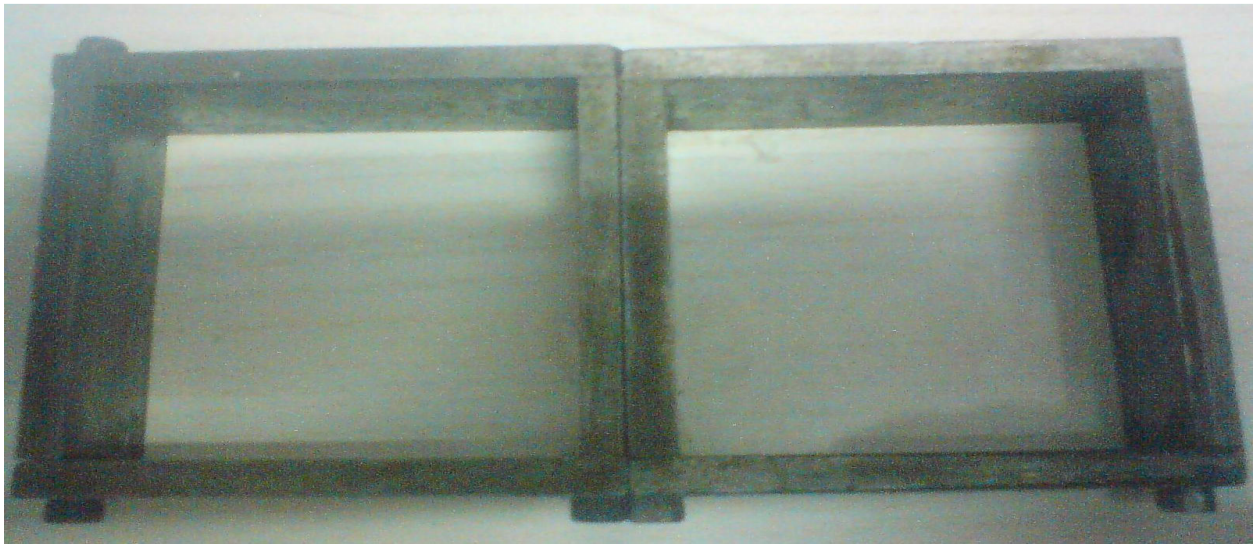

Figure 4.3: Mould for sample preparation of Direct Shear Test

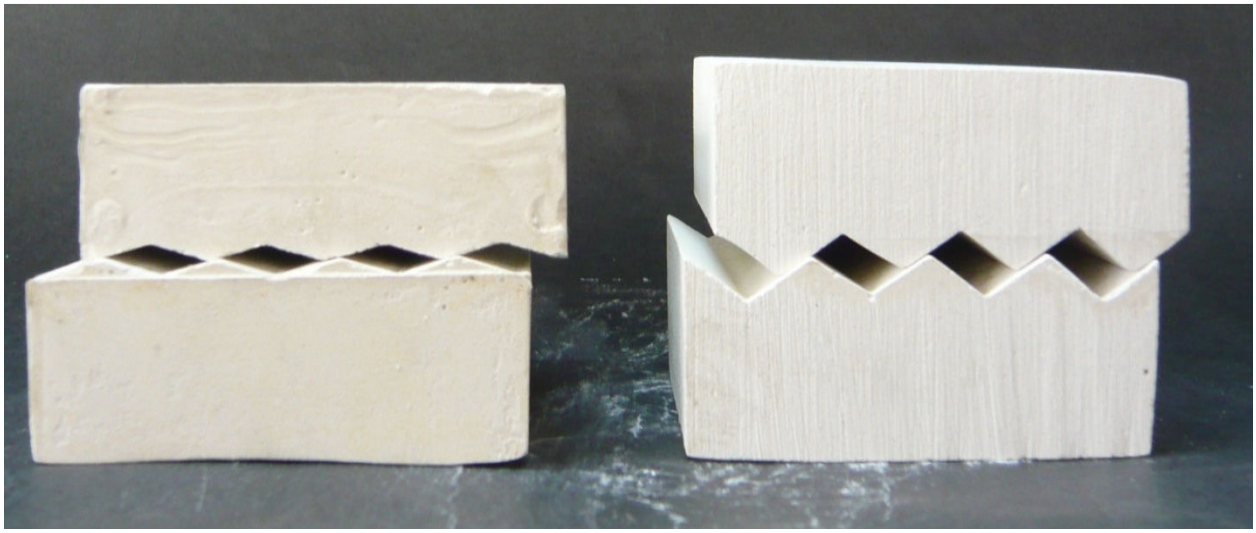

a) 15 -15 degree sample b) 30-30 degree sample

Figure 4.4: Direct Shear Test Sample

4.2. Material Characterization

4.2.1. Determination of Specific Gravity [IS 2720 –Part3]

Specific gravity of Plaster of Paris is determined according to IS 2720- Part3, using Le-Chatelier flask. Firstly weight of clean flask with its stopper is taken (W_1); than sample weighing approximately 50 gm is placed into the flask such that it is half filled and again weighed with its stopper (W_2); polar liquid (kerosene) is added to POP in flask till it is about half filled and mixed thoroughly with glass rod to remove entrapped, more kerosene is added with continuous stirring till it flush with graduated mark. Outside surface of flask is dried and weighed (W_3). Empty the flask, clean it and refill it with clean kerosene flush it with graduated mark, wipe outside and weigh (W_4).

$$\text{specific gravity} = \frac{W_1 - W_2}{(W_1 - W_2) - (W_3 - W_4) \times 0.79} \quad (40)$$

where, W_1=Weight of empty flask

W_2 = Weight of flask + Plaster of Paris

W_3= Weight of flask + Plaster of Paris+ Kerosene

W_4= Weight of flask+ Kerosene

The specific gravity of Plaster of Paris obtained by this procedure is **2.13.**

4.2.2 Determination of Initial and Final Setting Time [IS 4031(Part5):1988]

Determination of initial and final setting is very important for the molding in order to estimate the elapsed time between paste formation and initial hardening during the sample formation, as paste should be poured in the mould before initial setting and also sample should be taken out of the mould after final hardening.

Initial Setting time of cement is defined as the period elapsed between the time when the water is added to the cement and the time at which the needle of 1 mm² section fails to penetrate the test block to a depth of 5 + 0.5mm from the bottom of mould.

Final setting time of cement is defined as the period elapsed between the time when the water is added to the cement and the time at which the needle of is area 1mm² with 5mm diameter attachment, makes an impression on the test block, while the attachment fails to make an impression on the test block.

Initial and Final setting time of Plaster of Paris at 30%, 40%, 50% by weight is determined.

Water % by weight	Initial Setting Time (min)	Final Setting Time (min)
30	5.45	7.3
40	8.4	10.55
50	12.41	15.3

4.2.3. Particle Size Distribution

Particle size distribution has been found by sieving 200gm of Plaster of Paris through standard sieves of size 2.23, 1.18, 0.6, 0.212, 0.15, 0.075 mm using mechanical vibrator for about 10 minutes. Particle size distribution so found is shown in the graph below:

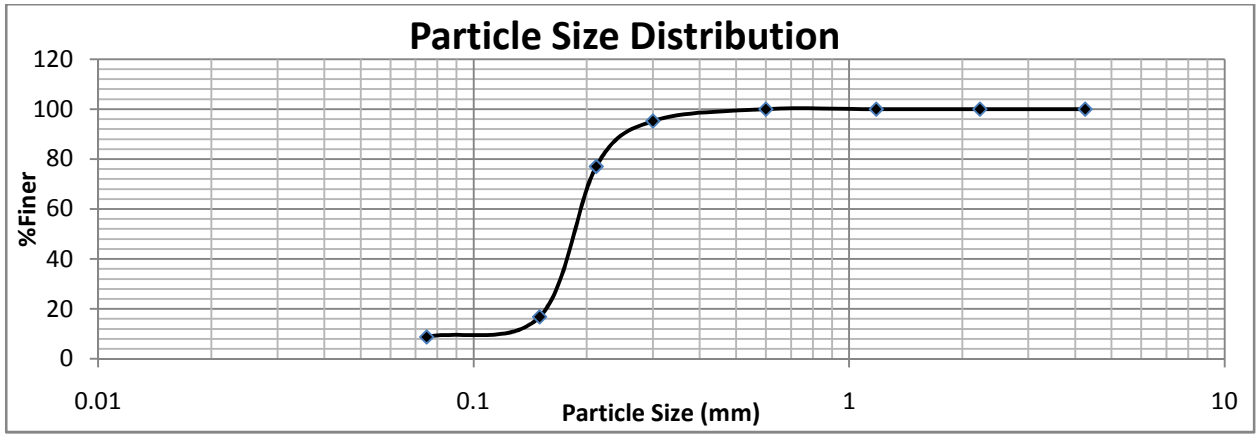

Figure 4.5: Particle Size Distribution Curve

4.2.4. UCS Test [7 Day And 14 Day]

In Uniaxial Compressive Strength test the cylindrical specimens were subjected to major principal stress till the specimen fails due to shearing along a critical plane of failure.

Perpendicularity of the axis were not deviated by 0.001radian and the specimen were tested after 7day and 14day.The prepared specimens (L=76 mm, D=38 mm) were put in between the two steel plates of the testing machine and load applied at the predetermined rate along the axis of the sample till the sample fails. The deformation of the sample was measured with the help of a separate dial gauge. During the test, load versus deformation readings were taken and a graph is plotted. When a brittle failure occurs, the proving ring dial indicates a definite maximum load which drops rapidly with the further increase of strain. The applied load at the point of failure was noted. The load is divided by the bearing surface of the specimen which gives the uniaxial compressive strength of the specimen.

Test was conducted on the samples prepared for 30%, 40%, 50% water content (by weight) of Plaster of Paris after 7 day curing and after 14 day on the sample of 50% water content.

Typical Stress-Strain Curve Obtained for Plaster Of Paris:

Figure 4.5 show the relationship obtained in Uniaxial Compressive Test conducted on samples of POP made by molding at 30%, 40% and 50% water by weight after 7 days of air curing.

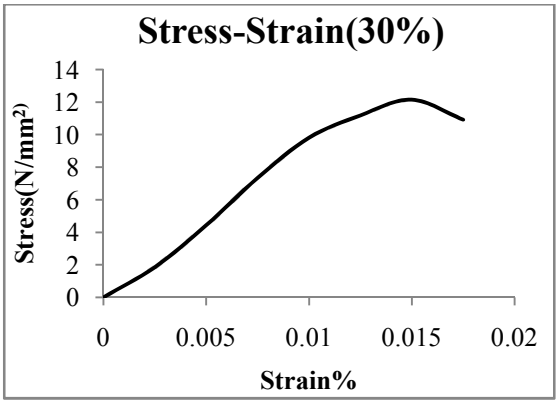

(a)

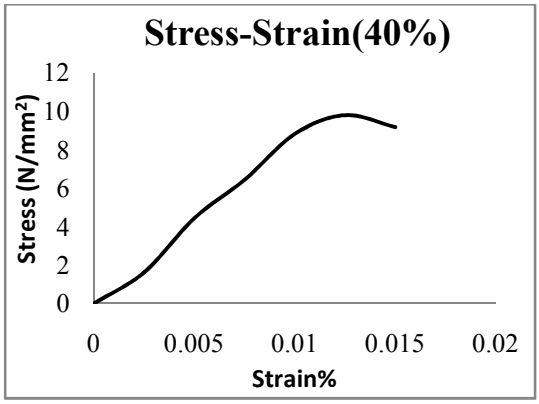

(b)

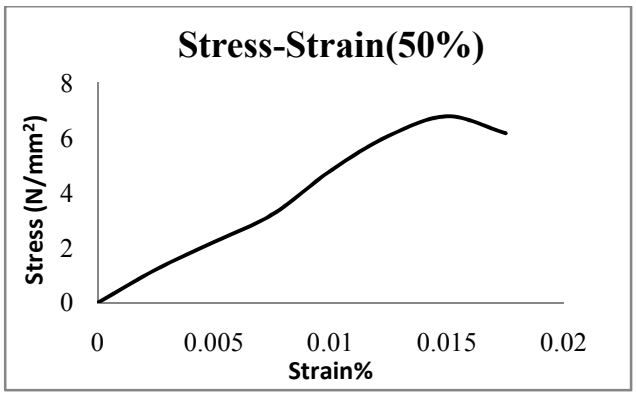

(c)

Figure 4.6: Typical Stress- Strain curve for (a) 30%; (b) 40%; (c) 50% water by weight.

Table 2 enlist the average value of maximum compressive strength which was shown by the POP samples for the three different water % after 7 day of curing

Table 2: Comparison of Compressive strength for different water content after 7 day curing

Water % by weight	UCS (N/mm^2)
30	12.15
40	9.79
50	6.65

Compressive strength for 50% water content after 14day curing: Uniaxial Compressive Strength of Plaster of Paris for 50% water content after 14 curing is **11.478MPa** and typical stress- strain relationship for the samples is shown in figure 4.6.

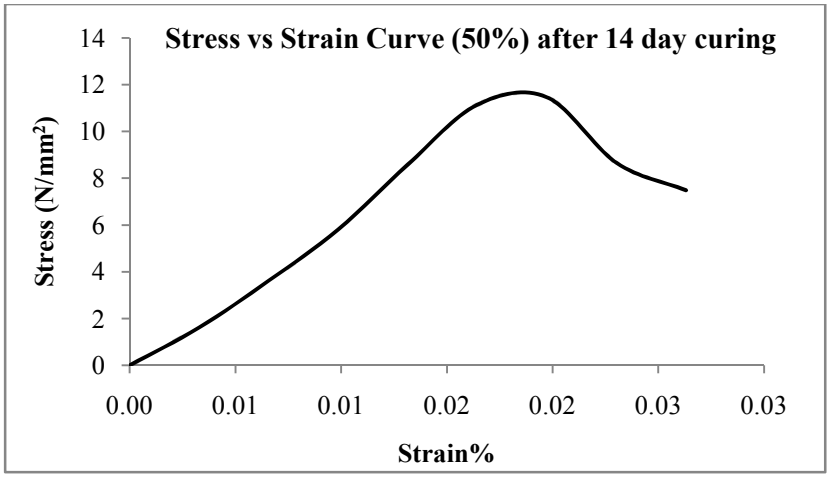

Figure 4.7: Typical Stress- Strain curve for 50% water by weight after 14 day curing

Typical failure pattern observed in Plaster of Paris:

Figure 4.7 and Figure 4.8 shows the cracking pattern shown by POP sample in UCS test. Former is for the 7 day cured sample (at 30%, 40%, 50% water) while later is for 50 % water molded sample cured for 14 days.

After 7day curing:

(a)

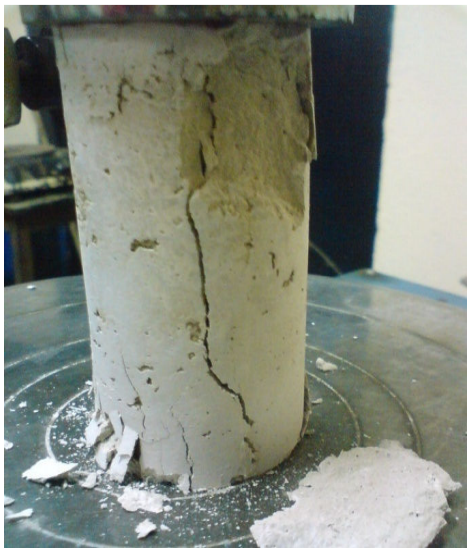

(b)

(c)

Figure 4.8: Failure Pattern Observed in samples (a) 30%; (b) 40%; (c) 50% water by weight

After 14day curing:

Figure 4.9: Failure Pattern Observed in samples for 50% water by weight after 14 day curing

4.2.5. Direct Shear Test 14day [IS 2720 Part 13-1986]

In order to study the shear behaviour of soft rock joints under constant normal load (CNL) tests is conducted on gypsum plaster joints of identical surface profiles. The plaster joint (in two halves) has been cast within the twin-box assembly as explained earlier.

In direct shear test, bottom box can move only in the horizontal direction, while the top box can move only in the vertical direction during shearing. Test has been conducted on various specimens of identical regular saw tooth profiles in the large shear apparatus under constant normal load. The test was conducted under normal stresses σ_n=.05, 0.1, 0.20, 0.5 and 1 N/mm^2.

During this test normal load is kept constant and shear resistance offered by joints due to interlocking, friction is measured. Test result, show the relationship between:

a) Shear stress vs. shear (horizontal) displacement

b) Dilation (vertical displacement) vs. shear (horizontal) displacement

4.2.5.1 Specification of Apparatus:

Direct shear test is carried out with an apparatus consisting of a square divide into two halves. The specimen, contained in the box is subjected to a constant normal load, while an increasing horizontal force is applied to one of the sections of the shear box. This force causes a shear failure along junction between the box sections. The shear and normal force are measured directly. Rate of strain is adjusted by the speed of the horizontal force applied. The loading unit has V-strips on which the shear box housing rests. Specimen of size 60x60x40mm can be tested.

Normal and shear displacement are measured with the help of 2 linear variable differential transducers (LVDT's) having range of ±20mm. The sensitivities of LVDT's are 0.025mm for shear displacement and 0.0025mm for normal displacement. Rate of strain can be varied from 0.002mm/min to 1.25mm/min. Apparatus consist of digital indicator and for display consist of micro-controller multi line VFD display. The Three-channel micro processor based signal conditioning unit is the three-function system. The functions are load, horizontal displacement and vertical displacement directly indicated in their respective engineering units. The system receives the output signal from the sensors i.e. Load cell and Displacement Sensors attached to the Direct Shear Test apparatus. Micro controller unit that stores the reading of each sensor finally transfers it to computer. The data of all three channels of Direct Shear Test can be transferred to computer and can be monitored online. The Unit also provides the facility of online monitoring of data through LCD display.

In general shear testing equipment consist of-

1. Shear box assembly, 60 mm square, complete with a U-bracket, guide pins and spacing screws, made of brass.

2. Gripper assembly consisting of two plain grid plates, two perforated grid plates, one base plate and one loading pad, all made of brass.
3. Two porous stones, each 6 mm thick, fitting the shear box
4. Shear box housing of brass, complete with two ball roller strips.
5. Loading unit with normal loading of 8kg/cm^2 on 60 mm square specimen.
6. Load cell universal (universal) 2kN- 1No.
7. LVDT ±20mm - 2 No.

Figure 4.10: Direct Shear Testing Equipment

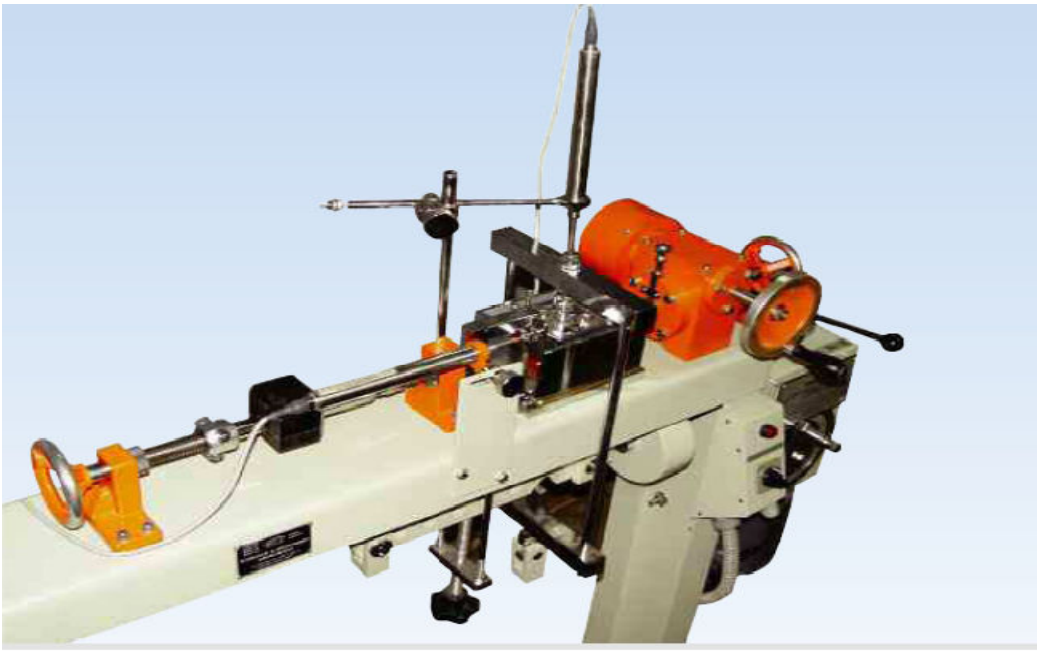

Figure 4.11: LVDT's and Loading frame in Direct Shear Test

(http://www.heicoin.com)

4.3. Results

Shear test was performed at five different normal stresses under constant normal load condition(CNL). The normal stresses are 0.05 N/mm^2, 0.1 N/mm^2, 0.2 N/mm^2, 0.25 N/mm^2 and 0.5 N/mm^2 and samples so tested are prepared with asperity angle 15° and 30° .

4.3.1 Comparison of Results at Different Normal Stress for Same Asperity Angle

Figure 4.13 and Figure 4.14 compare the shear behaviour of rock joint sample having same asperity angle but tested at different normal stresses. It can be easily observed that with the increase of normal stress both shear stress as well as dilation both is increases. Figure 4.12 shows the sheared sample of 15° and 30° asperity angle sample. In case of 15° substantial amount of breaking of tooth has not taken place, shearing is more likely to be simple sliping with crack formation from bottom while in case of 30° substantial amount of breaking of asperity tooth take

place due to high asperity angle and height and for shearing here in no longer easy and for shearing to take palce asperity breaking is must.

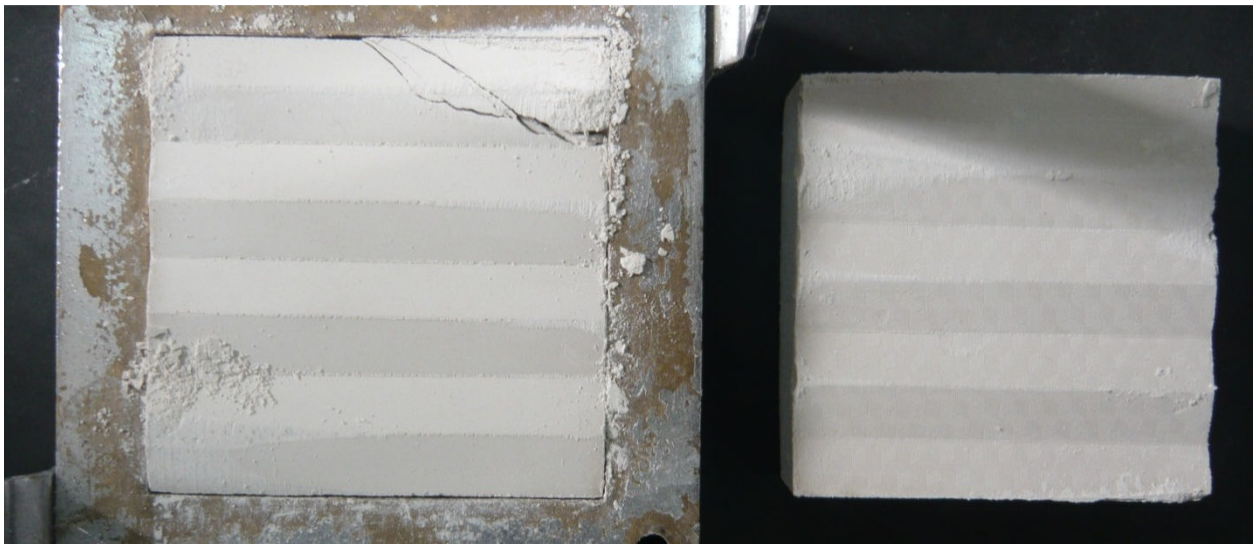

a) Sample of 15 degree asperity after shearing

b) Sample of 30 degree asperity after shearing

Figure 4.12: Direct Shear Samples After Shearing

For 15° Asperity Angle

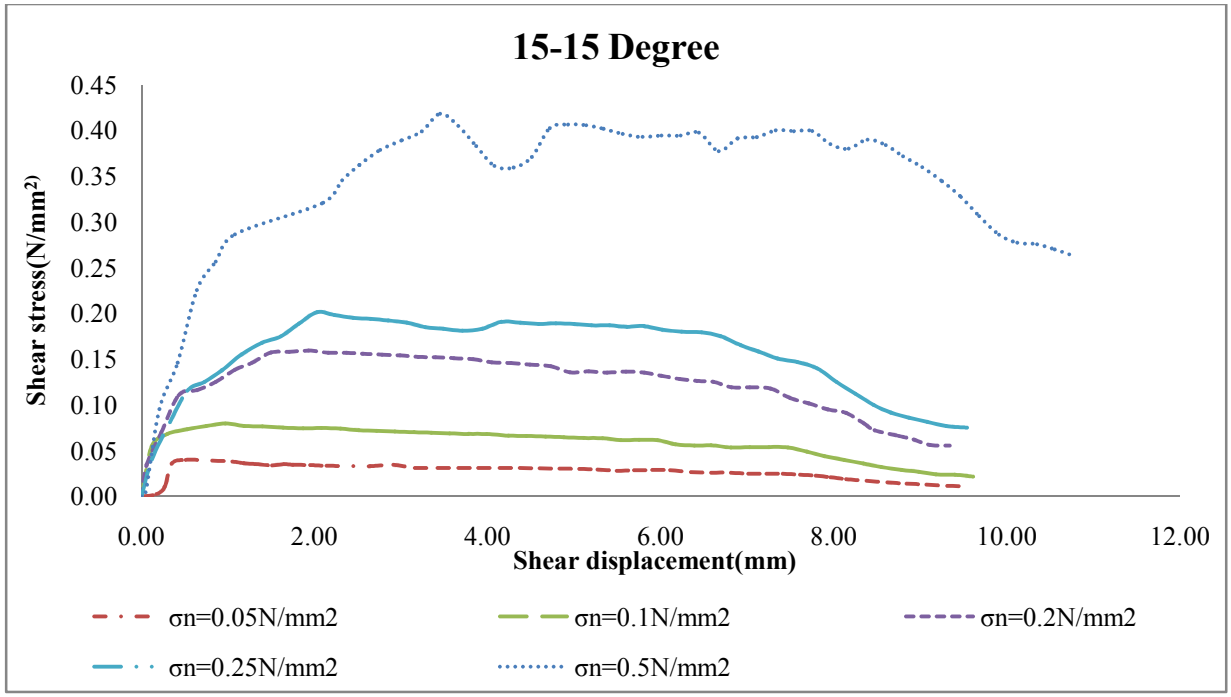

a) Shear Stress vs Shear Displacement

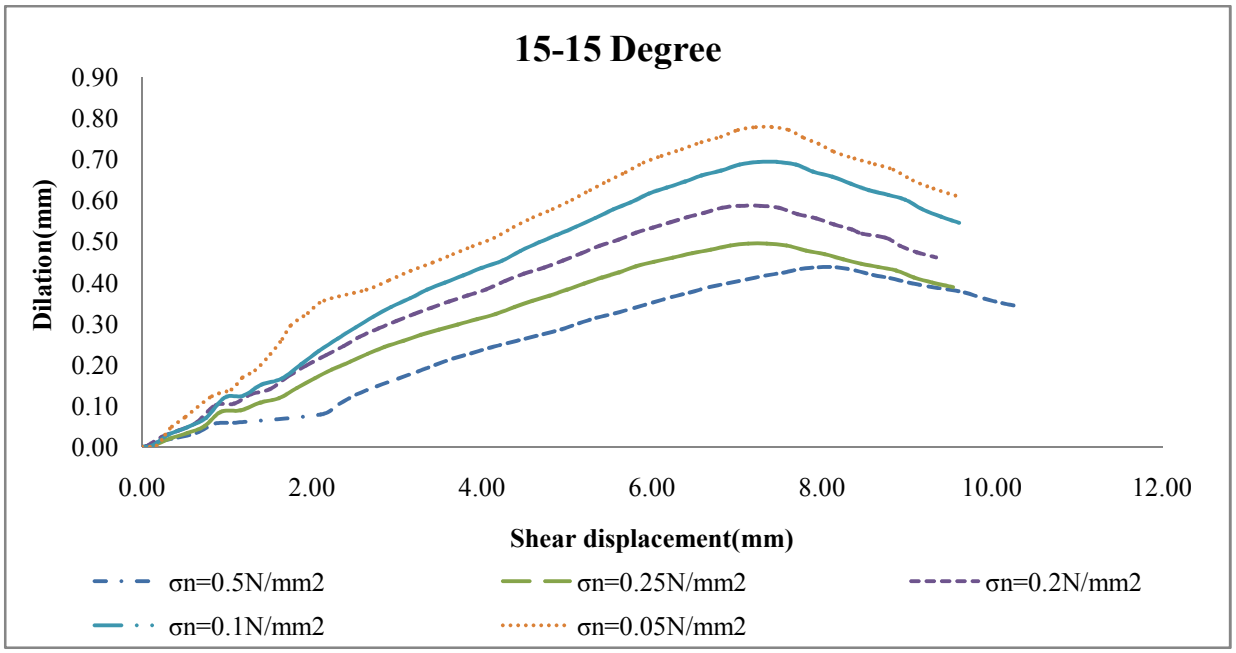

b) Dilation vs Shear Displacement

Figure 4.13 : Comparison of shear and dilation behaviour of 15° asperity samples at different Normal Stress

For 30◦ Asperity Angle

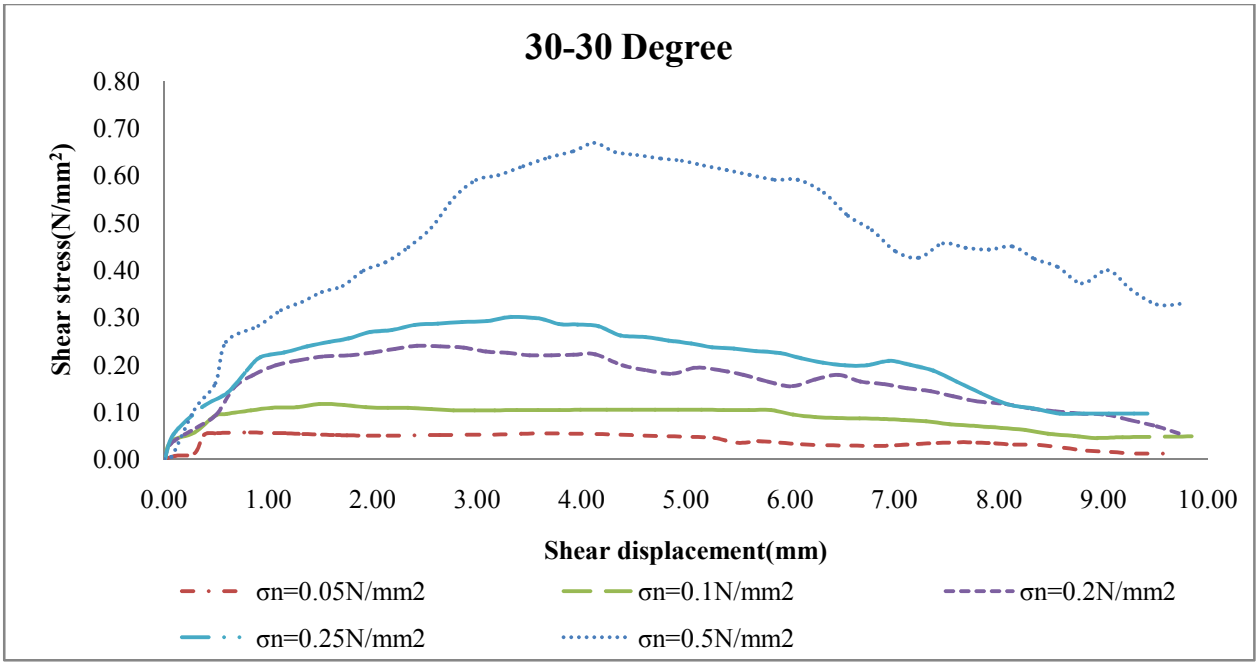

a) Shear Stress vs Shear Displacement

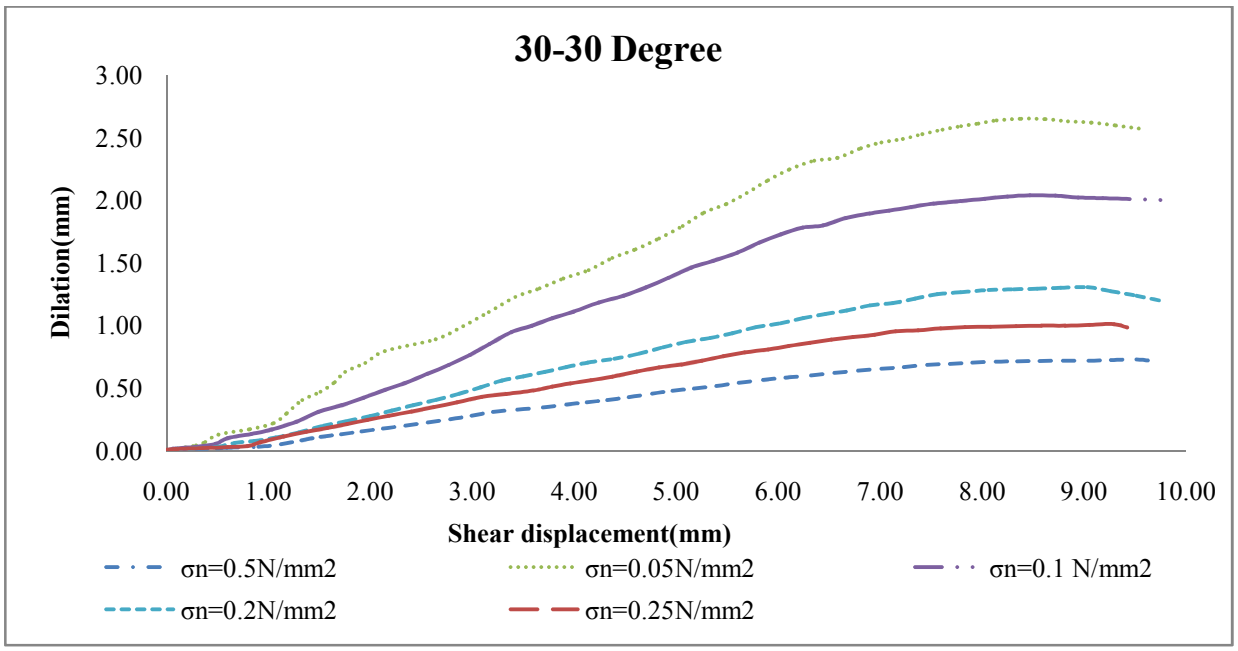

b) Dilation vs Shear Displacement

Figure 4.14 : Comparison of shear and dilation behaviour of 30° asperity samples at different normal Stress

4.3.2 Comparison of Results for Different Asperity Angle Joint Sample

Figure 4.15 compares the failure envelope obtained by plotting peak shear stress at different normal stress for 15° asperity angle sample with 30° asperity sample for CNL condition. Figure 4.16 compares the peak shear displacement of 15° asperity angle joint with that of 30° asperity angle at the same normal stress i.e. at σ_n = 0.05, 0.1, 0.2 , 0.25 and 0.5N/mm^2 respectively. Figure 4.17 compares peak secant dilation angle obtianed of 15° asperity angle joint with that of obtained for 30° asperity angle joint. From graphs it is very clear that peak shear stress, peak shear displacement as well as dilation(peak secant dilation angle) is increasing with increase in asperity angle . Peak shear stress and Peak shear displacement both increase with increase in normal stress while Peak secant dilation angle decrease with increase in normal stress.

Table 3: Experimental values obtained for 15° asperity sample

Normal stress σ_n (N/mm2)	Peak shear stress τ_p (N/mm2)	Peak shear dispalcemnt δ_p (mm)	Peak secant dilation angle $d_{t.peak}$ (◦)
0.05	0.040	0.51	8.18
0.1	0.079	0.97	7.06
0.2	0.159	1.93	5.85
0.25	0.201	2.03	4.70
0.5	0.418	3.45	3.32

Table 4: Experimental values obtained for 30° asperity sample

Normal stress σ_n (N/mm2)	Peak shear stress τ_p (N/mm2)	Peak shear dispalcemnt δ_p (mm)	Peak secant dilation angle $d_{t.peak}$ (°)
0.05	0.051	0.82	11.70
0.1	0.117	1.49	11.75
0.2	0.240	2.42	8.52
0.25	0.301	3.33	7.73
0.5	0.669	4.12	5.35

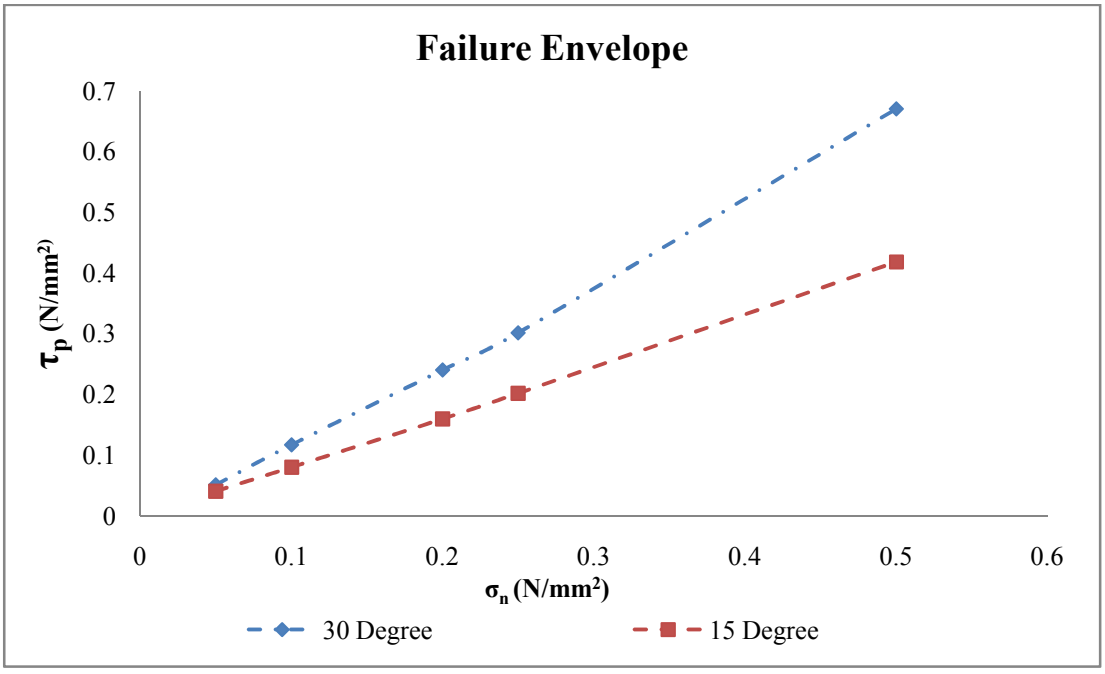

Figure 4.15 : Failure Envelope for Joints blocks

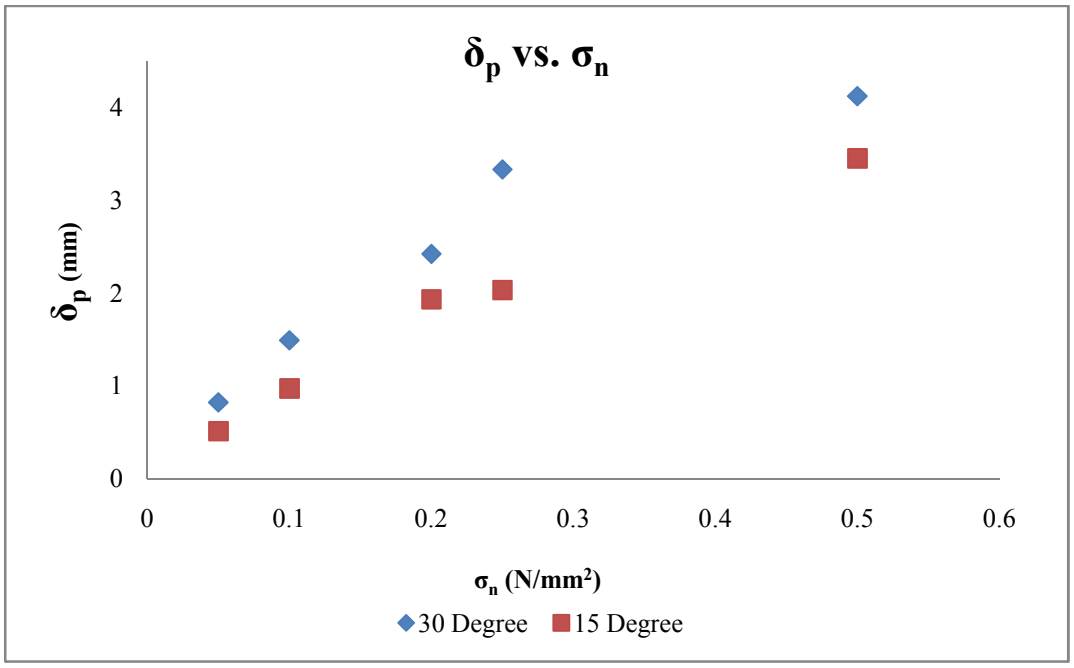

Figure 4.16: Comparison of Peak Shear Displacement for 15° and 30° asperity angle

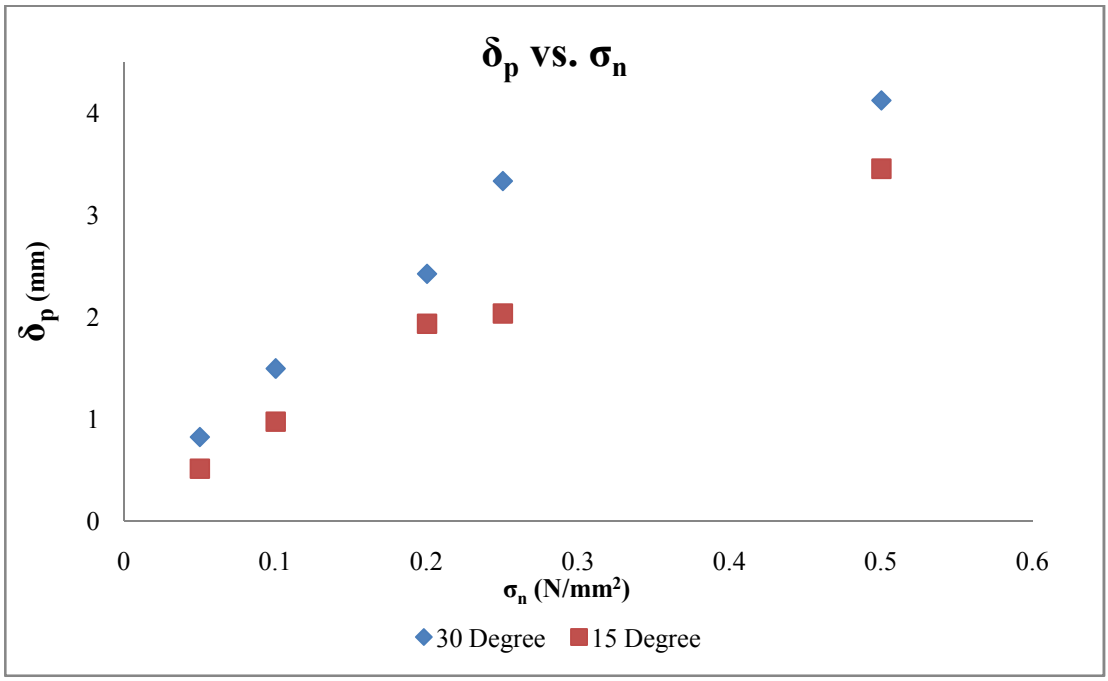

Figure 4.17: Comparison of Peak Secant Dilation angle for 15° and 30° asperity angle

4.3.3 Discussion on Experimental Results

Following points were observed after observing all the test results:

1) It was observed that the peak dilation angle decreases with increase in normal stress. This phenomenon is because of the resistance provided by the normal load against the dilation in joints.
2) The shear stress increases in jointed samples with increase in normal stress. It shows that the jointed rocks shows same variation in shear stress with change in normal stress as in normal soil.
3) An upward shift in peak shear displacement was observed with increasing normal stress. This could be due to the combined effort of shear stress as well as normal stress against dilation.
4) It was observed that peak dilation angle increases with increase in asperity angle at same normal stress. The height of asperity was more in 30 than 15 which provided that excess dilation in samples of larger asperity angles. Also the crushed material from first joint behaves like infill for the another joints.
5) The peak shear stress was more for larger asperity angle than the smaller one. The larger surface area of discontinuity in 30° angle than 15° angle is the reason for providing resistance against . Larger angles provide good interlocking conditions which further provides resistance against shear failure.
6) Peak shear displacement shows an incremental trend with increase in asperity angle at same normal stress. The reason behind is that the movement of joints is more in larger asperity angles at same failure points.

7) The post peak behaviour was observed in each of the tests was first increasing an than decresing. The phenomenon was observed further with continous increase in shear displacement. The reason behind is that the shear stress increases till the first joint breaks down. After that the shear stress falls immediately untill the joint shows dilation again for another set of joints. This phenomenon will continue till all the sets of joints broke down. Also the crused material from previous sets of joints behaves as infill material for another set of joints which reduces the peak dilation for another set of joints. Hence the overall shape of variation of dilation with shear displacement.

CHAPTER 5

NUMERICAL MODELLING

5.1 UDEC

The Universal Distinct Element Code (UDEC) is a 2-D numerical program based on the distinct element method for discontinuum modeling (discussed in chapter 2). UDEC can simulate the response of discontinuous media (such as a jointed rock mass) for both static as well as dynamic loading. In UDEC, discontinuous medium is represented as an assemblage of various discrete blocks, and discontinuities are treated as boundary conditions between blocks. Large displacements along discontinuities and rotations of blocks are allowed and individual blocks behave as either rigid or deformable material. Here deformable blocks are subdivided into a mesh of various finite-difference elements, and each element responds according to a prescribed linear or nonlinear stress-strain law; the relative motion of the discontinuities is also governed by linear or nonlinear force-displacement relations for movement in both the normal and shear directions. UDEC has several built-in material behavior models, for both the intact blocks and the discontinuities, which permit the simulation of response representative of discontinuous geologic, or similar, materials. UDEC is based on a "Lagrangian" calculation scheme that is well-suited to model the large movements and deformations of a blocky system. UDEC is command driven software but very easy to implement.

UDEC is primarily intended for analysis in rock mechanics projects, ranging from studies of the failure of rock slopes to evaluations of the influence of rock joints, faults, bedding planes, etc. on underground excavations and rock foundations. UDEC is ideally suited to study potential modes of failure directly related to the presence of discontinuous features. The program can best be used when the geologic structure is fairly well-defined — for example, from observation or geologic mapping. Both manual and automatic joint generator can be built into UDEC to create individual and sets of discontinuities which represent (in 2-D) jointed structure in a rock mass. A

wide variety of joint patterns can be generated in the model. A screen lotting facility allows the user to instantly view the joint pattern. Adjustments can be easily made before the final pattern is selected for analysis.

Different representations of joint material behavior are also available. The basic model is the Coulomb slip criterion, which assigns elastic stiffness, frictional, cohesive and tensile strengths, and dilation characteristics to a joint. A modification to this model is the inclusion of displacement weakening as a result of loss in cohesive and tensile strength at the onset of shear failure. A more complex model, the continuously yielding joint model, is also available and simulates continuous weakening behavior as a function of accumulated plastic shear displacement. As an optional feature, the Barton-Bandis joint model is also available at an additional cost. Joint models and properties can be assigned separately to individual, or sets of, discontinuities in a UDEC model. It should be noted that the geometric roughness of a joint is represented via the joint material model, even though the plot of discontinuities shows the joint as a straight-line segment. Blocks in UDEC can be either rigid or deformable. There are seven built-in material models for deformable blocks, ranging from the "null" block material (which represents holes-excavations), to the shear and volumetric yielding models (which include strain-hardening/softening behavior and represent nonlinear, irreversible shear failure and compaction). Thus, blocks can be used to simulate backfill and soil materials as well as intact rock. The basic formulation for UDEC assumes a 2-D plane-strain state. This condition is associated with long structures or excavations with constant cross-section acted on by loads in the plane of the cross section. Discontinuities, therefore, are considered as planar features oriented normal to the plane of analysis.

The explicit solution algorithm in UDEC permits either dynamic or static analysis. For dynamic calculations, user-specified velocity or stress waves can be input directly to the model either as an exterior boundary condition or interior excitation to the model. A library of simple dynamic wave forms is also available for input. UDEC contains non-reflecting and free-field boundary conditions for dynamic analysis.

Both stress (force) and fixed displacement (zero velocity) boundary conditions are available for static analysis. Boundary conditions may be different at different locations. In addition, a boundary element model is available to link to the UDEC model to simulate the boundary as an infinite elastic body. UDEC is able to simulate the flow of fluid through the discontinuities and voids in the model. A fully coupled mechanical-hydraulic analysis is performed in which fracture conductivity is dependent on mechanical deformation of the joint aperture; conversely, joint water pressures affect the mechanical behavior. Flow is idealized as laminar viscous flow between parallel plates. A visco-plastic flow model is also available to simulate flow of cement grout in the joints. There is also a thermal model available in UDEC. This model simulates the transient flux of heat in materials and the subsequent development of thermally induced stresses. The heat flux is modeled by either isotropic or anisotropic conduction. Heat sources can be added and can be made to decay exponentially with time.

UDEC contains a powerful built-in programming language, FISH, which enables the user to define new variables and functions. FISH is a compiler; programs entered via a UDEC data file are translated into a list of instructions stored in UDEC's memory space.

5.2. Continuously Yielding Joint Model

The deformability of the discontinuities between the blocks and their frictional characteristics in UDEC are modelled by spring slider system with prescribed force displacement relations

enabling the normal and shear forces between the blocks to be calculated. The UDEC contains three constitutive models for the joint. First is the Coulomb slip model which provides a linear representation of joint stiffness and yield limit. It is based upon elastic stiffness, frictional, cohesive, tensile strength properties and dilation characteristics common to rock joint. Second, continuously yielding model which is more realistic than the Coulomb joint model as it accounts for nonlinear behaviour observed in physical tests. This joint model, displays a continuous accumulation of plastic displacement from the onset of shearing. The instantaneous slope (i.e. tangent to the shear stress vs. shear displacement curve) is governed not only by the stiffness k, but also by the factor F. For a given shear displacement, F depends on the distance from the actual shear stress curve (τ) and the bounding strength curve (τ_m).

The continuously yielding joint model was proposed by Cundall and Hart in 1984, is intended to simulate, the internal mechanism of progressive damage of joints under shear in a simple fashion. The model also provides continuous hysteretic damping for dynamic simulations, by using a "bounding surface." The continuously yielding model is considered more "realistic" than the standard Mohr-Coulomb joint model in that the continuously yielding model attempts to account for some nonlinear behavior observed in physical tests (such as joint shearing damage, normal stiffness dependence on normal stress, and decrease in dilation angle with plastic shear displacement).

The essential features of the continuously yielding model include the following:

- The curve of shear stress/shear displacement is always tending toward a"target" shear strength for the joint—i.e., the instantaneous gradient of the curve depends directly on the difference between strength and stress.

- The target shear strength decreases continuously as a function of accumulated plastic displacement (a measure of damage).
- Dilation angle is taken as the difference between the apparent friction angle (determined by the current shear stress and normal stress) and the residual friction angle.

As a consequence of these assumptions, the model exhibits, automatically, the commonly observed peak/residual behavior of rock joints. Also, hysteresis is displayed for unloading and reloading cycles of all strain levels, no matter how small.

The model is described as follows. The response to normal loading is expressed incrementally as

$$\Delta\sigma_n = k_n \Delta u_n \tag{42}$$

where the normal stiffness, k_n, is given by

$$k_n = a_n \sigma_n^{e_n} \tag{43}$$

represents the observed increase of stiffness with normal stress, where a_n and e_n are model parameters. In general, zero tensile strength is assumed.

For shear loading, the model displays irreversible, nonlinear behavior from the onset of shearing. Figure 5.1 shows a typical stress-displacement curve for monotonic loading under constant normal stress. The shear stress increment is calculated as

$$\Delta\tau = F k_s \Delta u_s \tag{44}$$

where the shear stiffness, k_s , can also be taken as a function of normal stress

$$k_s = a_s \sigma_n^{e_n} \tag{45}$$

The bounding strength is given by

$$\tau_m = \sigma_n \tan \emptyset_{eff} \tag{46}$$

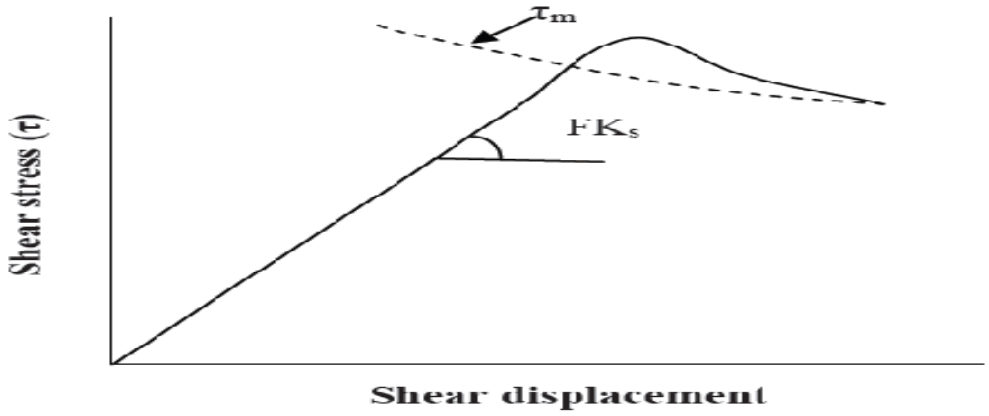

Figure 5.1: Shear stress- displacement curve and bounding shear strength (Itasca, 2004)

Where σ_n and ϕ_{eff} are normal stress and effective friction angle respectively. During the shearing process effective friction angle continuously reduced from ϕ_b + i to ϕ_b where, ϕ_b and i are the basic friction angle and initial angle of dilatancy respectively.

From Shrivastava, 2012 it has been observed that continuous yielding joint model was used for gives better prediction than other models for non-planar joint but it has limitation in predicting the peak shear stress at higher initial normal stress. He has also modified the CYM to consider the effect of CNS boundary condition and law of effective friction angle used in continuous yielding joint model (Shrivastava, 2011).

5.3. Modelling of Direct Shear Test in UDEC

Model geometry of size 60mmX60mmX40mm is created in UDEC software which is same as the laboratory specimen. The desired asperity is created for rock joint having asperity angle 15-15 and 30-30 with asperity height 2mm and 4.33mm respectively by crack command. The UDEC model of the sample is shown in Figure 5.2 (a) and Figure 5.2 (b).

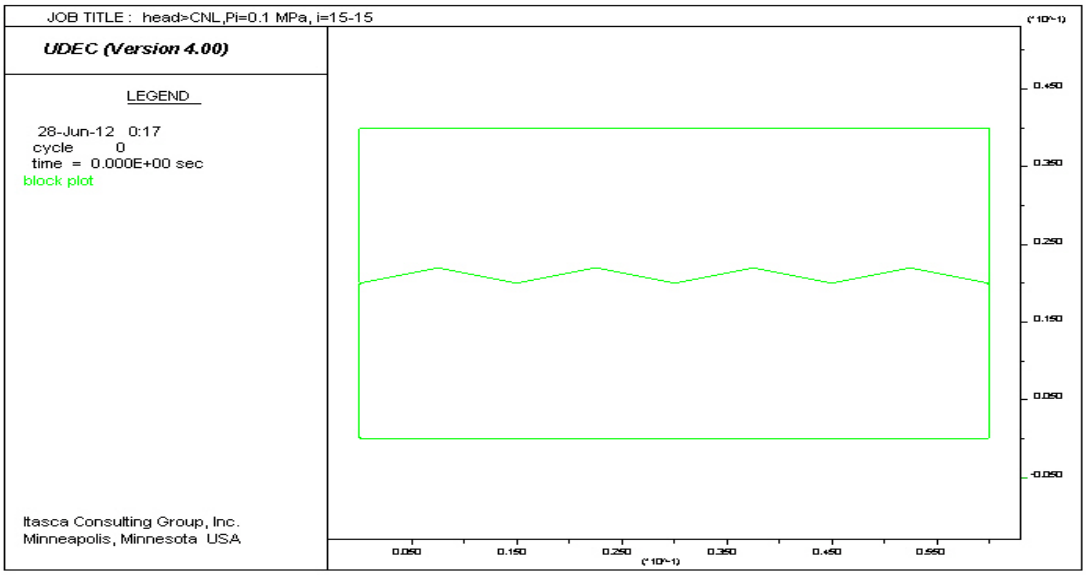

a) 15° asperity angle

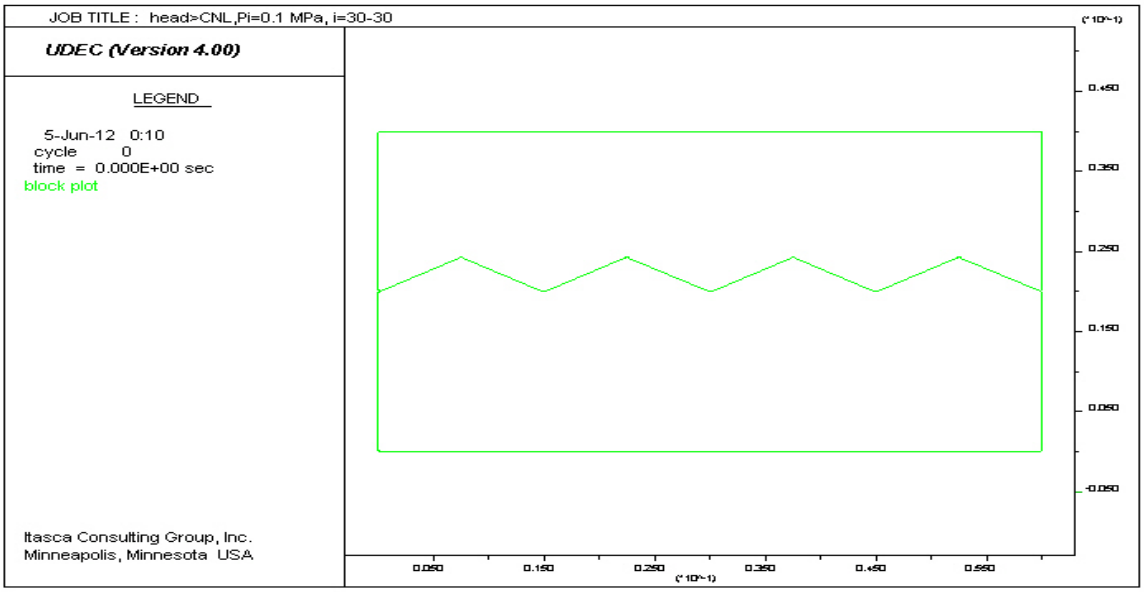

b) 30° asperity angle

Figure 5.2: Blocks created by UDEC

Table 5: Continuously yielding model properties for direct shear tests (Shrivastava et.al, 2012)

Property key word	Description	Value
D	Block mass density	1234kg/m^3
K	Bulk modulus of block	1.357 GPa
G	Shear modulus of block	0.934 GPa
jkn	Joint normal stiffness	0.8 GPa/m
jks	Joint shear stiffness	0.8 GPa/m
jen	Joint normal stiffness exponent	0
jes	Joint shear stiffness exponent	0
jfric	Joint intrinsic friction angle	38.5°
jif	Joint initial friction angle	38.5+ asperity angle
jr	Joint roughness parameter	0.01mm

The properties of the material and the joint used for UDEC analysis is given in Table 3. These properties for numerical simulation are taken from Shrivastava et.al. 2012 as model material is same. A proper joint roughness parameter (jr) is selected, as it controls the rate at which effective friction angle decreases with plastic shear displacement. A smaller value of jr causes effective friction angle to decrease rapidly, which is resulting into smaller peak stress. Initial boundary condition is applied on the sample in such a way that the lower shear box is only allowed to move in X direction and movement in Y direction is restricted by imposing Y velocity at the bottom of the lower shear box as zero. The upper shear box is allowed to move only in the Y direction and movement in the X direction is restricted by imposing X velocity at the sides of the

Upper shear box as zero. The boundary conditions are similar to the conditions used during laboratory testing. Initial normal stress at the top of the sample is applied for CNL. The model is run for large number of cycles to reach equilibrium and give desired shear displacement to the sample. At equilibrium, the force on one side of a grid point nearly balances the opposing force. The sample is then sheared by imposing the shear velocity on the lower sample. It has been observed during analysis that the asperity degradation cannot be modeled properly by continuously yielding joint model of UDEC, because of the over prediction of the dilation of the joint and hence over prediction of the corresponding normal stress. Under conventional CNL, the asperity degradation is less prominent at the same initial normal stress and at similar shear displacement; hence UDEC predictions are more appropriate for CNL than CNS conditions.

5.4 Comparison of Experimental and UDEC Result

Numerical simulation of joint using UDEC was done and results are compared with those obtained experimentally for same normal stress and same asperity angle. It has been found that UDEC predict quite near to experimental values. Hence UDEC can be used for predicting the jointed rock behaviour in the absence of any experimental result and also where obtaining and testing of sample is difficult.

For Asperity angle 15°

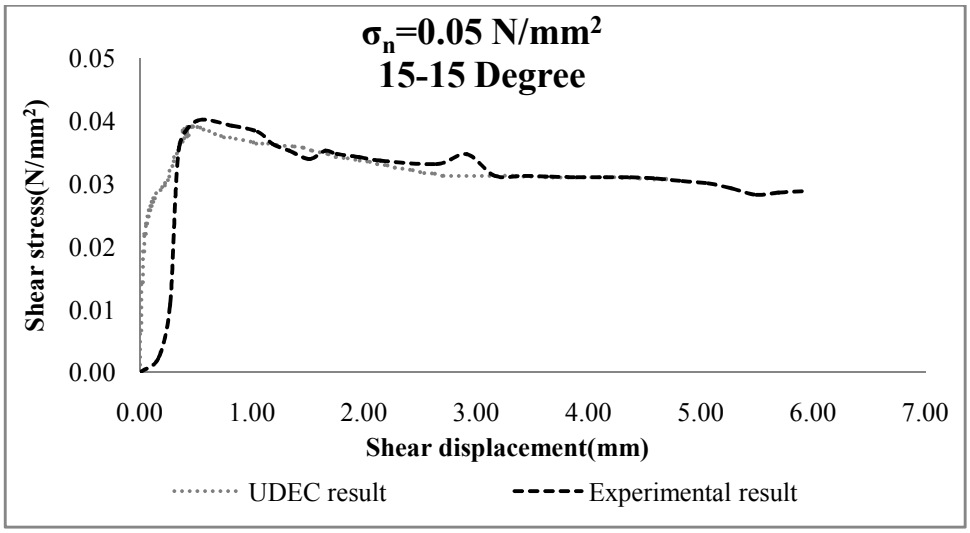

Figure 5.3: Comparison of Experimental result with UDEC for 15° asperity angle at σ_n=0.05MPa

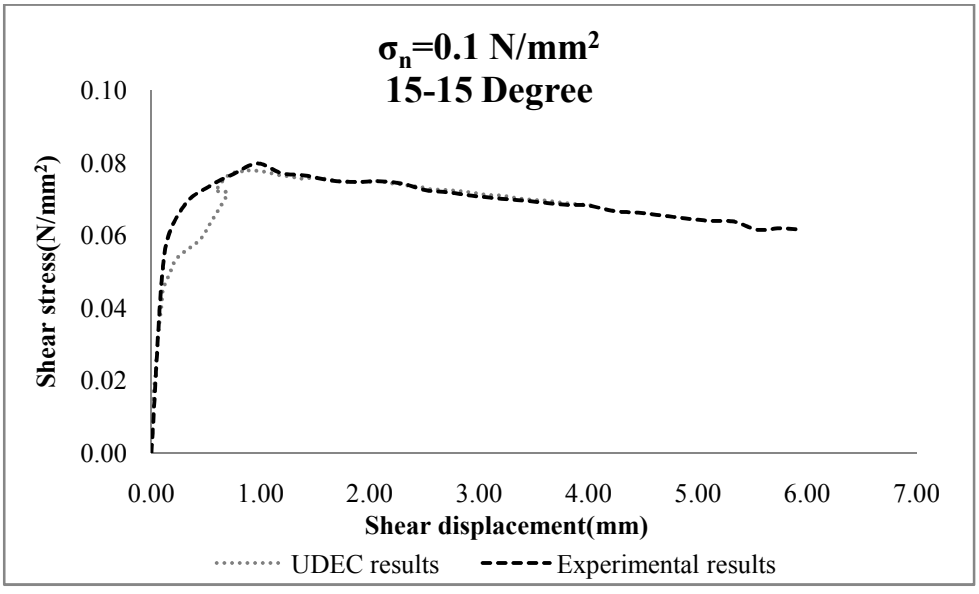

Figure 5.4: Comparison of Experimental result with UDEC for 15° asperity angle at σ_n=0.1MPa

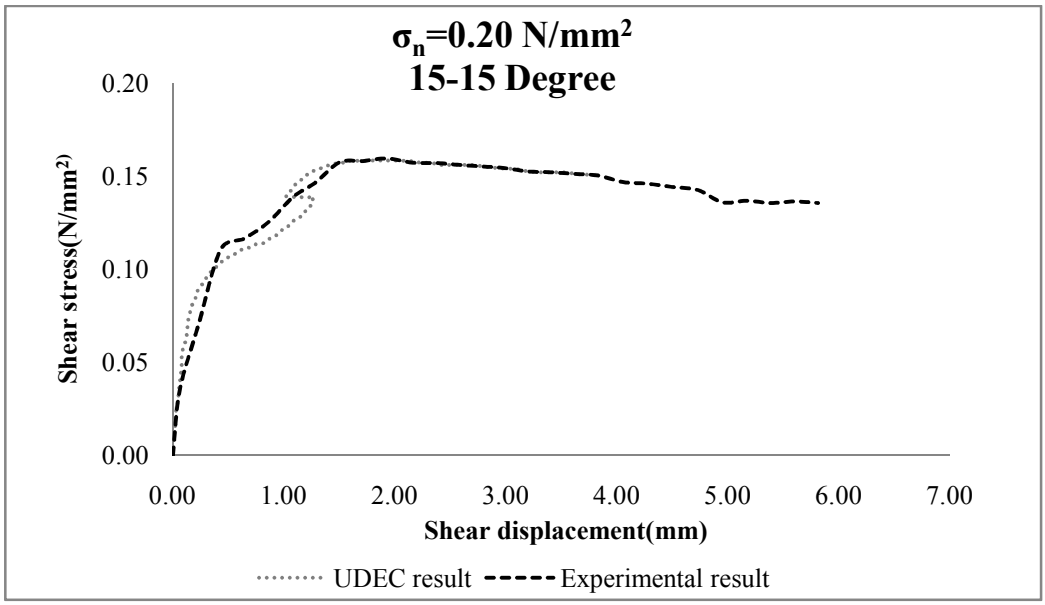

Figure 5.5: Comparison of Experimental result with UDEC for 15° asperity angle at σ_n=0.2MPa

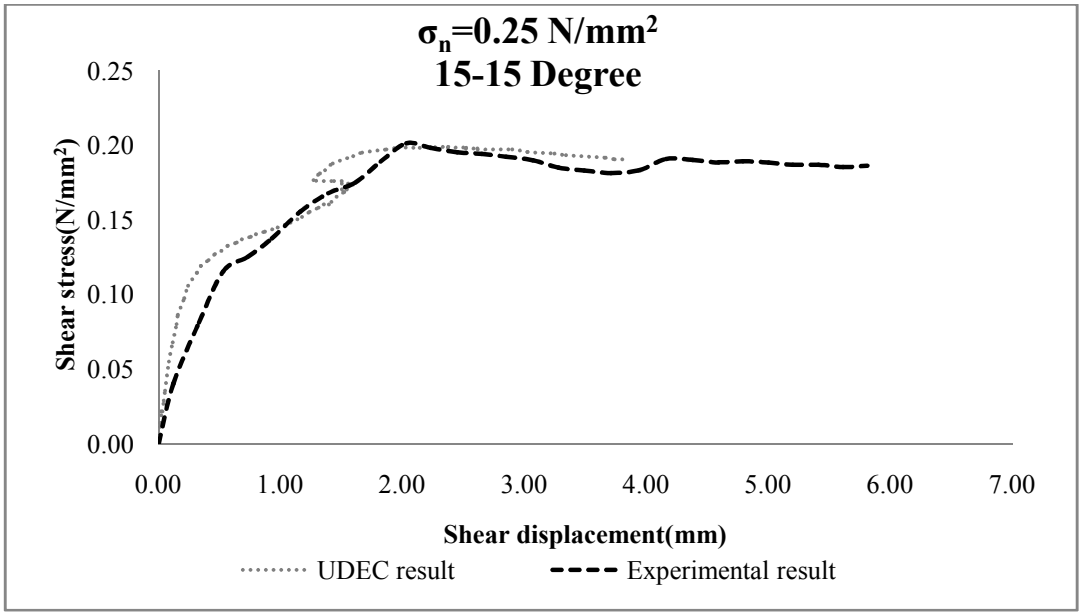

Figure 5.6: Comparison of Experimental result with UDEC for 15° asperity angle at σ_n=0.25MPa

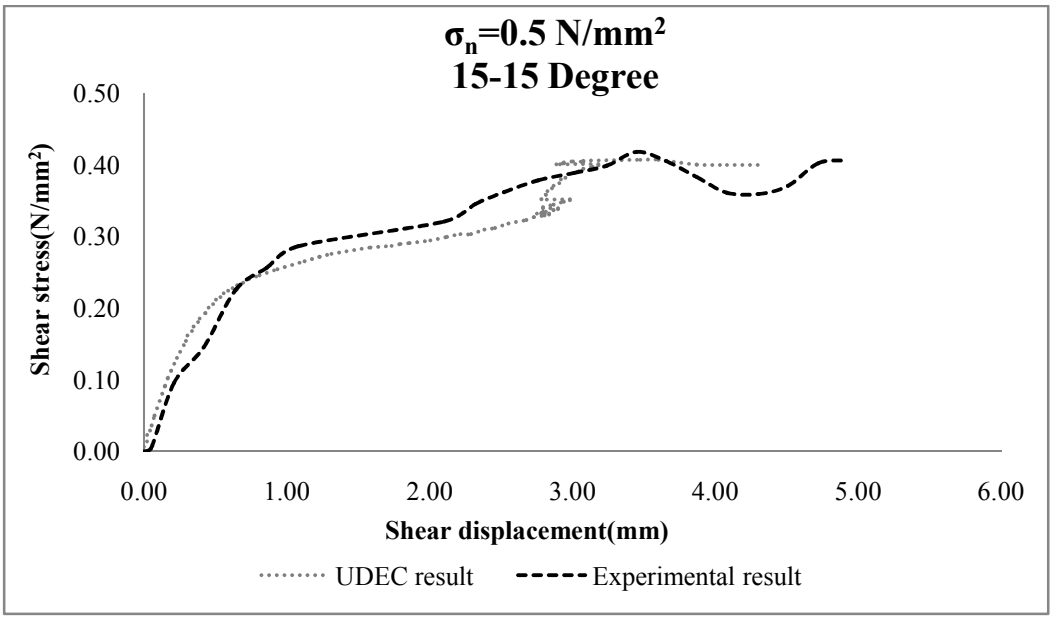

Figure 5.7: Comparison of Experimental result with UDEC for 15° asperity angle at σ_n=0.5MPa

For Asperity angle 30°:

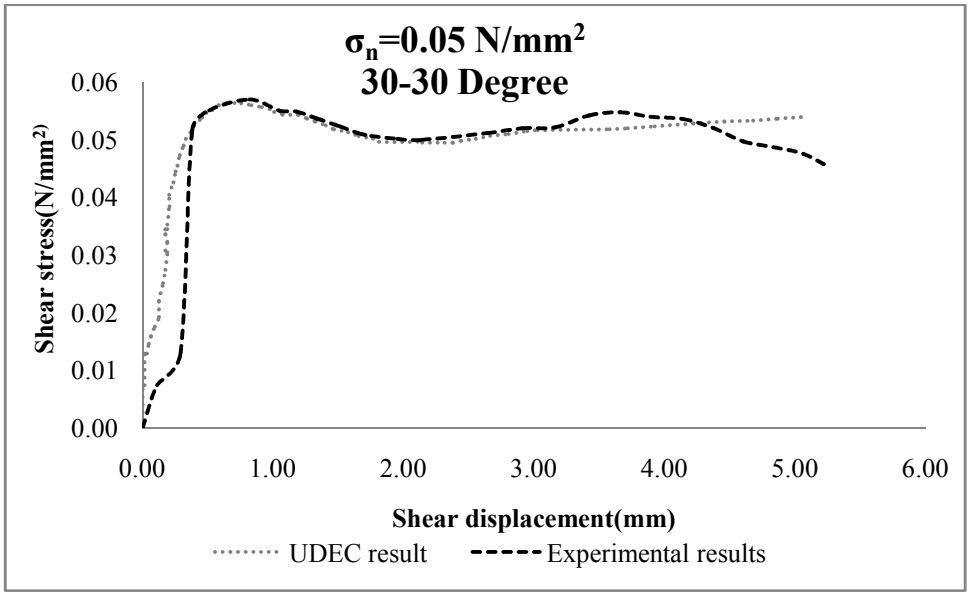

Figure 5.8: Comparison of Experimental result with UDEC for 30° asperity angle at σ_n=0.05MPa

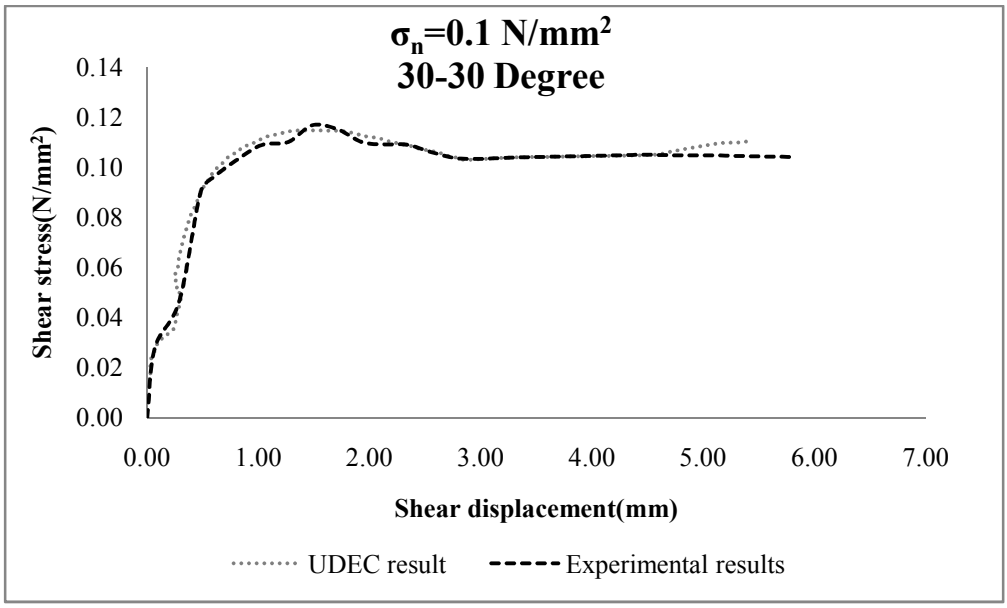

Figure 5.9: Comparison of Experimental result with UDEC for 30° asperity angle at σ_n=0.1MPa

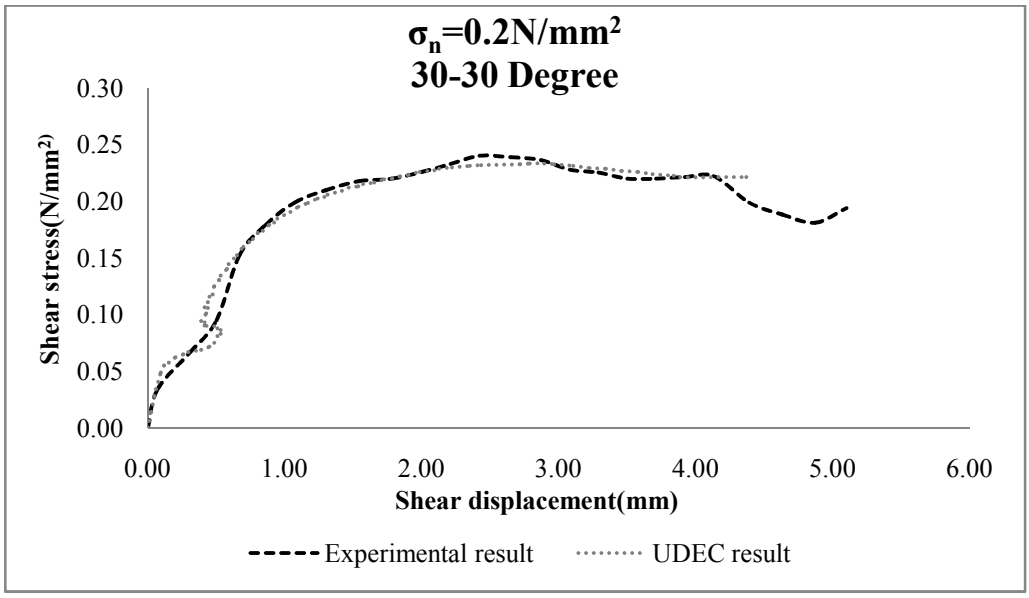

Figure 5.10: Comparison of Experimental result with UDEC for 30° asperity angle at σ_n=0.2MPa

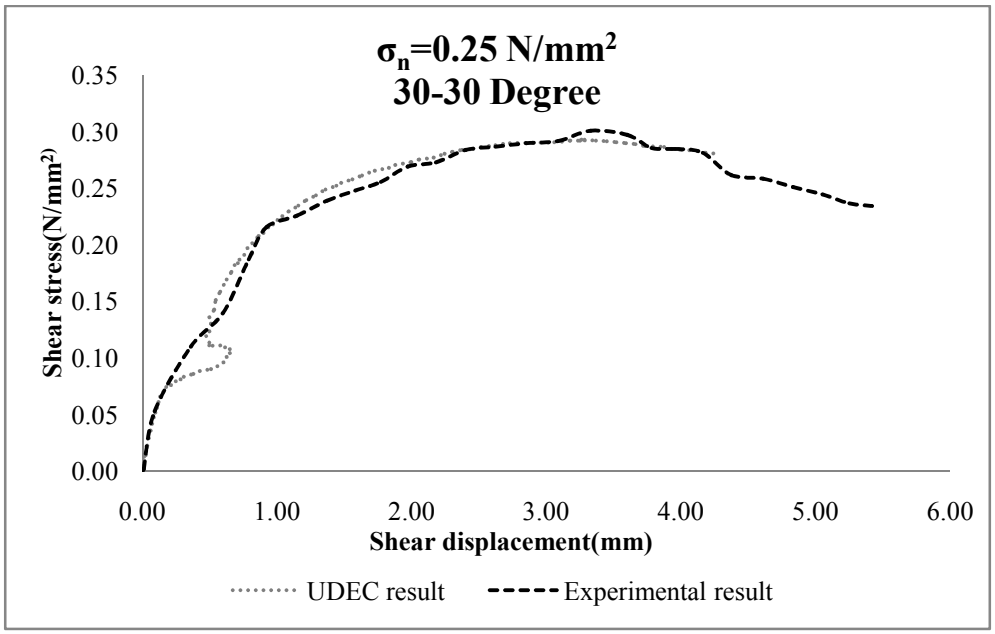

Figure 5.11: Comparison of Experimental result with UDEC for 30° asperity angle at σ_n=0.25MPa

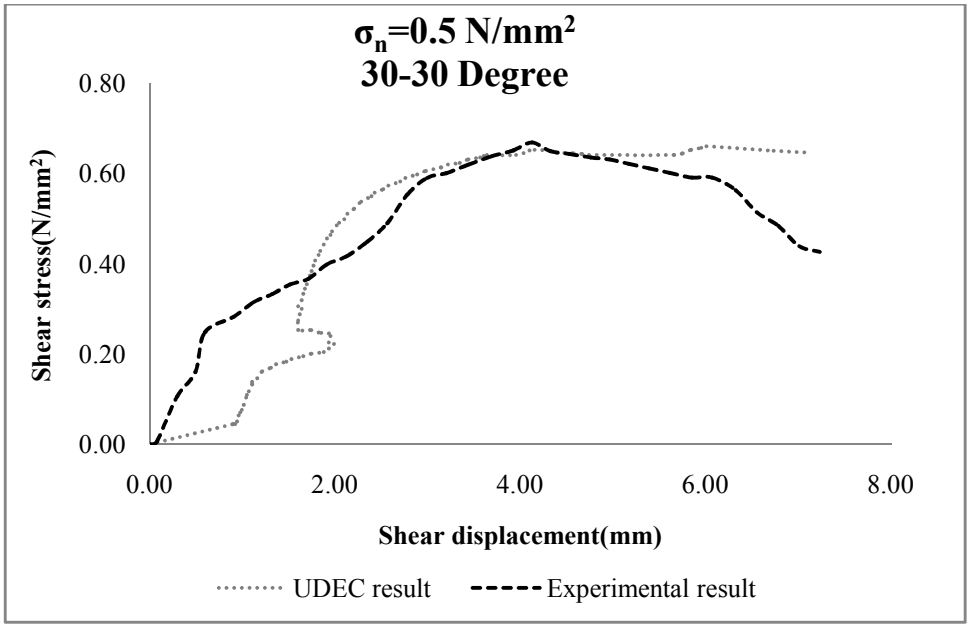

Figure 5.12: Comparison of Experimental result with UDEC for 30° asperity angle at σ_n=0.5MPa

5.5 Comparison of results with that of obtains using well known equation

1) Peak Shear Stress: Comparison is done between experimental result and the result obtain by using UDEC, using Barton's Equation, 1973 (equation no. 6) and Patton's Equation, 1966 (equation no. 1). From the figure 5.13 and figure 15.4, it can be easily concluded that Barton's Eqn. and Patton's Eqn. are over predicting the peak shear stress, while peak shear stress predicted by UDEC is in close agreement with experimental result. Though at lower normal stress these criteria can be used but at higher normal stress there applicability decreases.

Table 6: Value of Peak Shear Stress obtained for 15° angle

Normal Stress σ_n (N/mm^2)	Experimental values of τ_p (N/mm^2)	UDEC values of τ_p (N/mm^2)	Patton's Eqn. of τ_p (N/mm^2)	Barton's Eqn. of τ_p (N/mm^2)
0.05	0.040	0.039	0.07	0.07
0.1	0.079	0.075	0.14	0.14
0.2	0.159	0.158	0.27	0.25
0.25	0.201	0.198	0.34	0.31
0.5	0.418	0.407	0.68	0.57

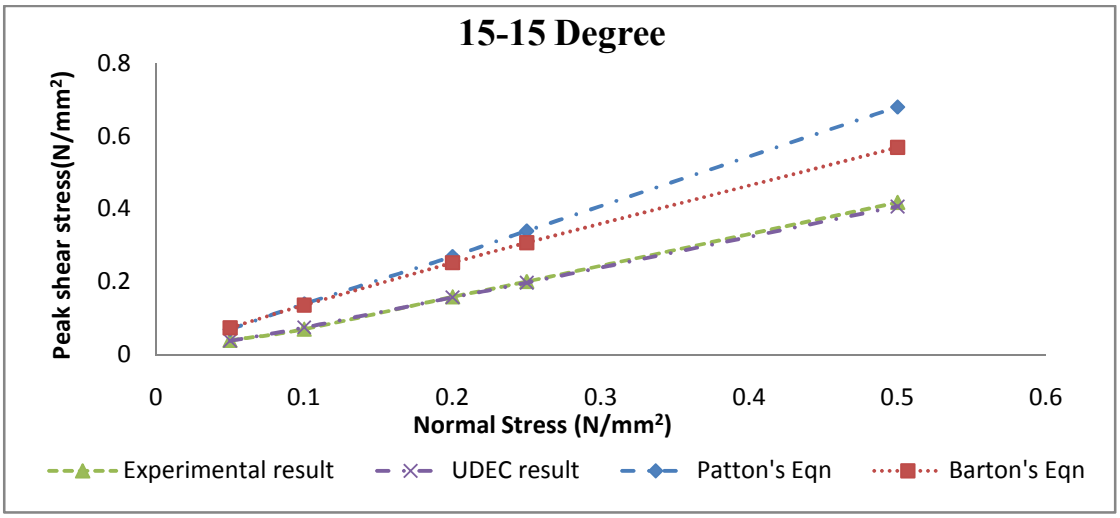

Fig 5.13: Comparison of Experimental Peak Shear Stress with the results of UDEC, Barton's Eqn. and Patton's Eqn. for 15° asperity angle

Table 7: Value of Peak Shear Stress obtained for 30° angle

Normal Stress σ_n (N/mm^2)	Experimental values of τ_p (N/mm^2)	UDEC values of τ_p (N/mm^2)	Patton's Eqn. of τ_p (N/mm^2)	Barton's Eqn. of τ_p (N/mm^2)
0.05	0.051	0.056	0.13	0.16
0.1	0.117	0.114	0.25	0.27
0.2	0.240	0.233	0.51	0.43
0.25	0.301	0.293	0.63	0.50
0.5	0.669	0.660	1.27	0.83

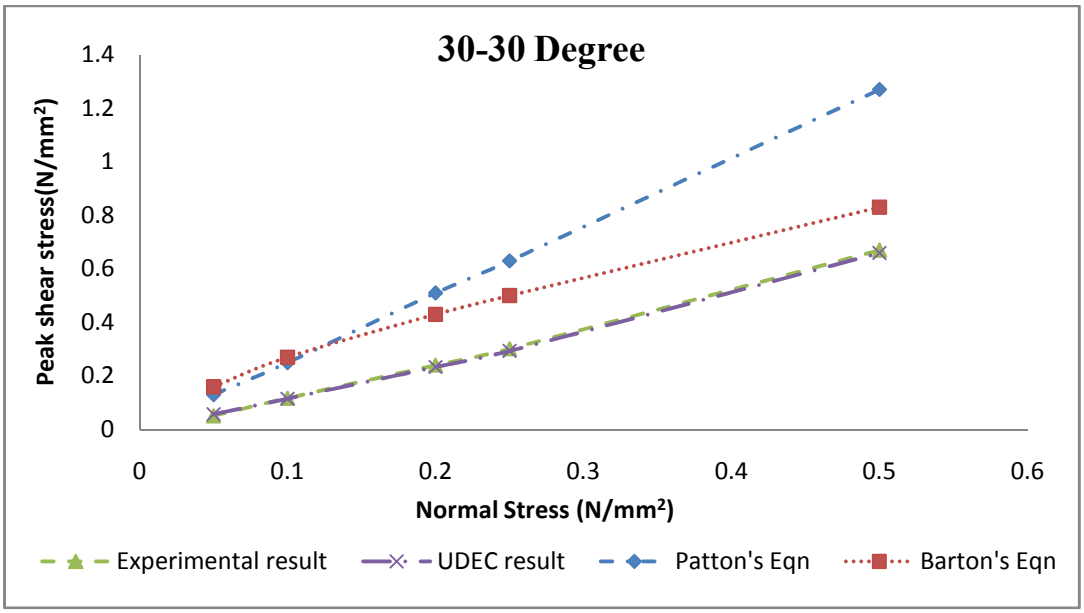

Figure 5.14: Comparison of Experimental Peak Shear Stress with the results of UDEC, Barton's Eqn. and Patton's Eqn. for 30° asperity angle

2) Peak Shear Displacement: Comparison is done between experimental result and the results obtain by using UDEC, using Barton-Bandis Equation, 1981 (equation no.21) and Asadollahi's Equation 2010 (equation no. 22). UDEC over predict peak shear displacement but when compared with the equation given by Bandis and Asadollahi, UDEC is found to predict more nearer to experimental value. As Bandis's equation has a serious problem as it does not consider the effect of normal shear on shear displacement while it has been found that shear displacement increase with increase in normal stress

Table 8: Value of Peak Shear displacement obtained for 15° angle

Normal Stress σ_n (N/mm^2)	Experimental values of δ_p (mm)	UDEC values of δ_p (mm)	Barton-Bandis Eqn. of δ_p (mm)	Asadollahi's Eqn. of δ_p (mm)
0.05	0.51	0.50	0.59	0.30
0.1	0.97	1.50	0.59	0.38
0.2	1.93	2.41	0.59	0.49
0.25	2.03	3.02	0.59	0.53
0.5	3.45	3.48	0.59	0.67

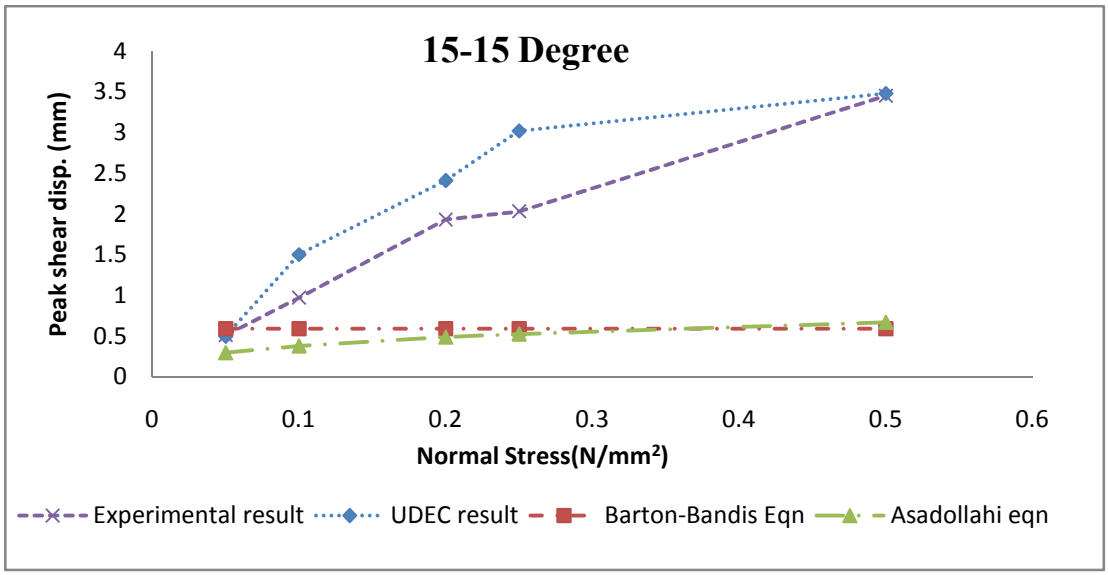

Figure 5.15: Comparison of Experimental Peak Shear Displacement with the results of UDEC, Barton-Bandis Eqn. and Asadollahi's Eqn. for 15° asperity angle.

Table 9: Value of Peak Shear displacement obtained for 30° angle

Normal Stress σ_n (N/mm^2)	Experimental values of δ_p (mm)	UDEC values of δ_p (mm)	Barton-Bandis Eqn. of δ_p (mm)	Asadollahi's Eqn. of δ_p (mm)
0.05	0.82	0.65	0.74	0.25
0.1	1.49	1.35	0.74	0.34
0.2	2.42	2.79	0.74	0.45
0.25	3.33	3.26	0.74	0.49
0.5	4.12	6.01	0.74	0.63

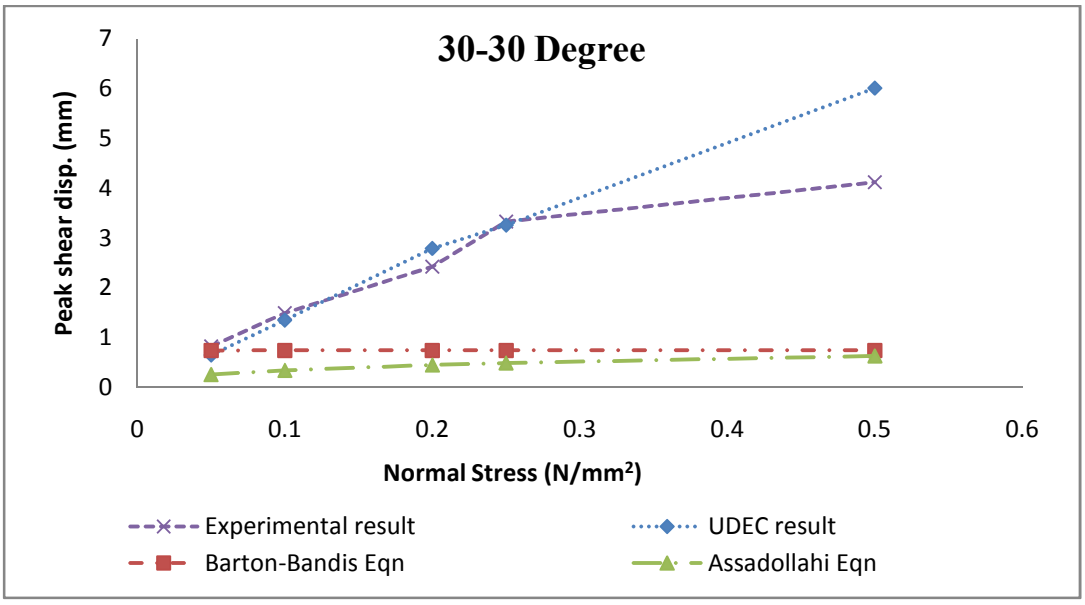

Figure 5.16: Comparison of Experimental Peak Shear Displacement with the results of UDEC, Barton-Bandis Eqn. and Asadollahi's Eqn. for 30° asperity angle.

3) Peak Dilation Angle: Comparison is done between experimental result and the results obtain by using Barton's Equation (equation no. 10) and Asadollahi's Equation (equation no. 19)

Table 10: Value of Peak Dilation angle obtained for 15° angle

Normal Stress σ_n (N/mm^2)	Experimental values of $d_{s.peak}$ (◦)	Barton's Eqn. of $d_{s.peak}$ (◦)	Asadollahi's Eqn. of $d_{s.peak}$ (◦)
0.05	8.18	5.90	6.07
0.1	7.06	5.15	5.26
0.2	5.85	4.39	4.47
0.25	4.70	4.15	4.21
0.5	3.32	3.40	3.43

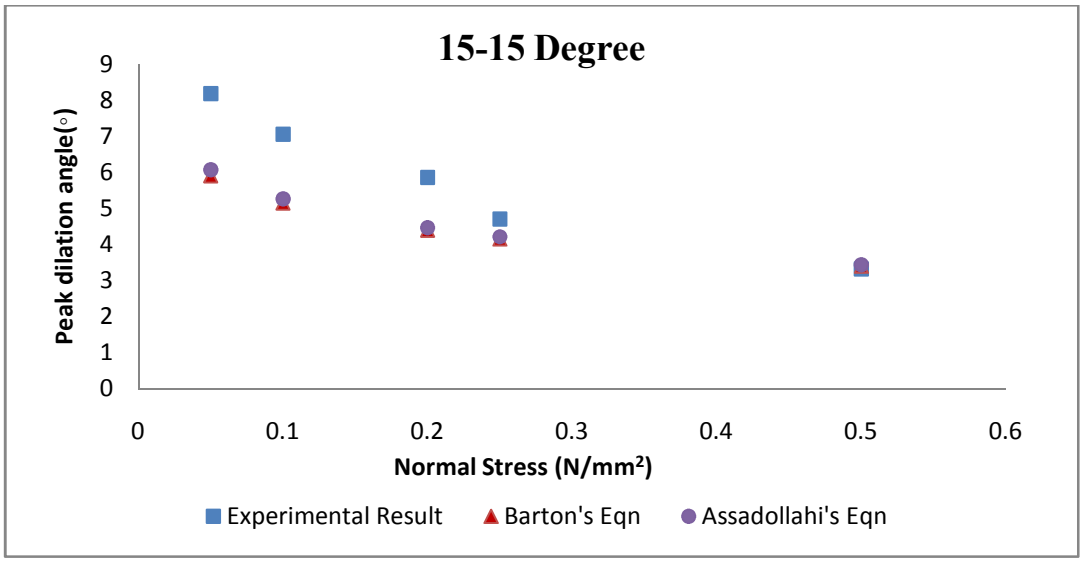

Figure 5.17: Comparison of Experimental Peak dilation angle with the results of Barton's Eqn. and Asadollahi's Eqn. for 15° asperity angle

Table 11: Value of Peak Dilation angle obtained for 30° angle

Normal Stress σ_n (N/mm^2)	Experimental values of $d_{s.peak}$ (◦)	Barton's Eqn. of $d_{s.peak}$ (◦)	Asadollahi's Eqn. of $d_{s.peak}$ (◦)
0.05	11.70	11.80	13.33
0.1	11.75	10.29	11.28
0.2	8.52	8.79	9.38
0.25	7.73	8.31	8.81
0.5	5.35	6.80	7.07

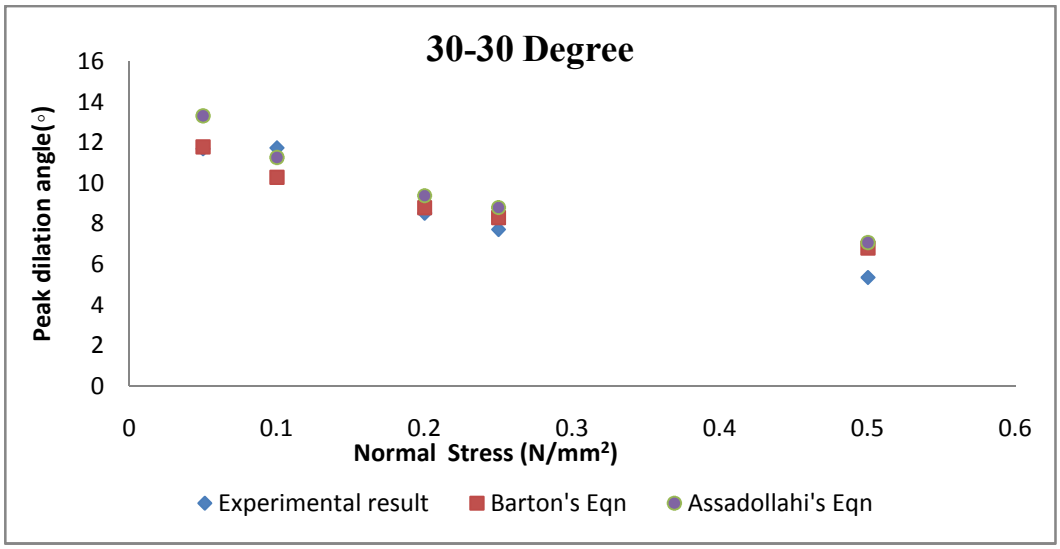

Fig 5.18: Comparison of Experimental Peak dilation angle with the results of UDEC, Barton-Bandis Eqn and Asadollahi's Eqn for 30° asperity angle.

CHAPTER 6

CONCLUSION

From the experimental and UDEC results following inferences can be made:

1) Peak shear stress increases with asperity angle and normal stress. This is due to the fact that greater asperity angle provides good interlocking condition and at higher normal stress greater force is to be applied in order to overcome internal resistance and cause sliding.
2) Peak secant dilation angle increases with asperity angle and asperity height but decreases with increase in normal stress. Also post-peak dilation value decrease with increase in normal stress
3) Peak shear displacement not only increases with increase in normal stress for same asperity angle joints but also show increasing pattern with increase in asperity angle for same normal stress.
4) Peak shear stress predicted using UDEC code is in close agreement with laboratory results. UDEC generally predict better at lower normal stress, but it decreases with increase normal stress. Although it has been noted that results predicted by UDEC are better than those obtain by using criteria proposed by Patton, 1966 and Barton, 1973.
5) UDEC also predict better results for peak shear displacement when compared with the famous equation given by Barton – Bandis , 1981 and Asadollahi, 2010.

CHAPTER 7

SCOPE FOR FUTURE WORK

This study was only concerned with shear behaviour of rock joints under CNL condition and this study can be extended to interpret behaviour of rock joints under CNS condition, as CNS condition is more realistic for non-planar in which one asperity over-rides each other and if surrounding rock is unable to deform then normal stresses increase inevitably and condition no longer remain CNL and become CNS.

Shear behaviour can also be checked in case of irregular joint having different asperity angle and for joints containing infill material as infill material highly effect the shearing pattern in rock-joints and hence test should be perform by using different infill material in order study the effect of infill or gauge material on behaviour of joint.

There is need of one criterion which can predict comparable to experimental values hence in further study large amount of test can be performed in order to generate equations that are capable of correctly predicting peak shear stress, peak shear displacement and peak dilation.

REFERENCES

1. Amadei, B., Saeb, S., 1990. "Constitutive models of rock joints". International Symposium on Rock Joints. A.A. Balkema, Leon, Norway.
2. Asadollahi, P., Tonon F. 2010. "Constitutive model for rock fractures: Revisiting Barton's empirical model". Engineering Geology, 11-32
3. Asadollahi, P., Tonon F., Invernizzi, M.C.A, Addotto, S. 2010, "experimental validation of modified Barton's model for rock fractures" Rock Mech Rock Eng.
4. Bandis, S.C., Lumsden, A.C. and Barton, N., 1981. "Experimental studies of scale effects on the shear behaviour of rock joints". 18: 1–21.
5. Bandis, S.C., Lumsden, A.C., Barton, N.R., 1983. "Fundamentals of rock joint deformation" Int. J. Rock Mech. Min. Sci. & Geomech. Abstr. 20 (6), 249–268.
6. Barla, G., Barla, M. 1999, "Continuum And Discontinuum Modelling In Tunnel Engineering", Scientific Symposium Rock Mechanics and Tunnelling, Zagreb, Croatia.
7. Barton, N., 1972." A model study of rock joint deformation". Int. J. Rock Mech. Min. Sci. 9, 570–602.
8. Barton, N., 1973. "Review of a new shear strength criterion for rock joints". Eng. Geol. 7, 287–332.
9. Barton, N., 1976." Rock mechanics review: the shear strength of rock and rock joints".Int. J. Rock Mech. Min. Sci. & Geomech. Abstr. 13, 255–279.
10. Barton, N., Bakhtar, K., 1983. "Rock Joint Description and Modelling for the Hydrothermomechanical Design of Nuclear Waste Repositories". Terra Tek Engineering.
11. Barton, N., Choubey, V., 1977. "The shear strength of rock joints in theory and practice" Rock Mech. 10, 1–54.

12. Barton, N., Bandis, S.C., Bakhtar, K., 1985. "Strength, deformation and conductivity coupling of rock joints". Int. J. Rock Mech. Min. Sci. & Geomech. Abst. 22 (3), 121–140.
13. Beer G, Meck J. L.,1981, "Infinite domain elements", International Journal Numerical Methods Eng, 17(1): 43–52.
14. Beer G., 1985. "Finite element, boundary element and coupled analysis of unbounded problems in elastostatics", Int J Numer Methods Eng, pp 67–80.
15. Bobet, A., Fakhimi, A., Johnson, S., Morris, J., Tonon F. and Yeung, M.R., 2009, "Numerical Models in Discontinuous Media: Review of Advances for Rock Mechanics Applications", Journal Of Geotechnical And Geoenvironmental Engineering , ASCE / November .
16. Brady, BHG, Wassyng A., 1981, "A coupled finite element—boundary element method of stress analysis", Int J Rock Mech Min Sci Geomech Abst ,pp. 475–85.
17. Cundall, P.A., Hart, R.D., 1992. "Numerical modelling of discontinua". Eng Comput; 9:101–13.
18. Cundall PA., 1985, "UDEC—a generalized distinct element program for modelling jointed rock". Report PCAR-1-80, Peter Cundall Associates, European Research Office, US Army Corps of Engineers
19. Desai, C.S., Fishman, K.L., 1987. "Constitutive models for rocks and discontinuities (joints)". 28th US Symp. on Rock Mechanics, Tuscon, pp. 609–619.
20. Borst, R., 2002, "Fracture in quasi-brittle materials: A review of continuum damage-based approaches", Eng. Fract. Mech., pp. 95–112.

21. Bieniawski Z.T, 1984, "Rock Mechanics Design in Minning and Tunneling", A.A. Balkema/Rotterdam/Boston.
22. Goodman, R.E., 1974. "The mechanical properties of joints". Proc. 3rd Congress. ISRM, Vol. 1A, p. 127–140, Denver, pp. 127–140.
23. Indraratna, B. (1990). "Development and application of a synthetic material to simulate soft sedimentary rocks." Geotechnique, Vol. 40, No. 2, pp. 189-200.
24. Indratna, B., Haque, A. and Aziz, N., 1998, "Laboratory modelling of Shear behaviour of soft joints under CNS condition", Geotechnical and Geological Engineering, pp.17-44.
25. Jing, L. and Hudson A, 2002, "Numerical Methods In Rock Mechanics", International Journal of Rock Mechanics & Mining Science, pp. 409–427.
26. Jing, L. 2003, "A Review Of Techniques, Advances And Outstanding Issues In Numerical Modelling For Rock Mechanics And Rock Engineering", International Journal of Rock Mechanics & Mining Sciences 40, pp. 283–353.
27. Jing, L., Stephansson, O., Nordlund, E., 1993. "Study of rock joints under cyclic loading conditions". Rock Mech. Rock Engng. 26 (3), 215–232.
28. Ladanyi, B., Archambault, G., 1969. Simulation of the shear behaviour of a jointed rock mass. The 11th Symposium on Rock Mechanics, Berkeley, pp. 105–125.
29. Lorig L J, Brady BGH, 1984, "A hybrid computational scheme for excavation and support design in jointed rock media", Proceedings of the Symposium Design and Performance of Underground Excavations. Cambridge: British Geotechnical Society, pp.105–12.
30. Maksimovic, M., 1996, "The shear strength components of a rough rock Joint". Int J Rock Mech Min Sci Geomech Abstr 33, pp.85–200.

31. Olsson, R., Barton, N., 2001. "An improved model for hydromechanical coupling during shearing of rock joints." Int. J. Rock Mech. Min. Sci. 38, 317–329.
32. Patton, F.D., 1966a. "Multiple modes of shear failure in rock". The 1st Congress of the International Society of Rock Mechanics, Lisbon, pp. 509–513.
33. Perrone N, Kao R. A., 1975, "General finite difference method for arbitrary meshes". Comput Struct , pp. 45–58.
34. Rao, K.S. and Shrivastava, A.K., 2011, "Shear behaviour of rock under CNL and CNS condition." Indorock, IIT Roorkee, pp.13-24.
35. Roosta, R.M., Mohammad, H.S., Ali, P. and Yaser, S., 2006, "Rock joint modeling using a visco-plastic multilaminate model at CNL condition", Geotechnical and Geological Engineering, pp. 1449-1468.
36. Shi, G. H., and Goodman, R. E., 1984, "Discontinuous deformation analysis." Proc., 25th U.S. Symposium on Rock Mechanics, Society of Mining Engineers of AIME, New York, 269–277.
37. Shi, G. H., and Goodman, R. E. 1985. "Two dimensional discontinuous deformation analysis." Int. J. Numer. Analyt. Meth. Geomech. 9, pp.541–556.
38. Shi, Goodman, 1988, "Discontinuous deformation analysis—A new numerical model for the statics and dynamics of block systems." Ph.D. thesis. Univ. of California, Berkeley, Calif.
39. Shrivastava, A.K., Rao K.S., and Rathod, G.W., 2012, "Numerical Simulation of Direct Shear Test on Rock-Joint" GSP, ASCE, pp. 2177-2186.
40. Tse R., Cruden, D.M., 1979, "Estimating joint roughness coefficients". Int J Rock Mech Min Sci Geomech Abstr 16:303–307.

41. Xie, H., Pariseau, W.G., 1992, "Fractal estimation of the joint roughness coefficients". In: Proceedings of international conference on fractured and jointed rock masses, Balkema, Rotterdam, pp.125–131.
42. ITASCA Consulting Group, Inc. UDEC Manual, 2004.
43. ITASCA Consulting Group, Inc. 3DEC Manual, 2004.